Theoretical rheo-physics of silk: Intermolecular associations reduce the critical specific work for flow-induced crystallisation

Charley Schaefer[1, a)] and Tom C. B. McLeish[1]

Department of Physics, University of York, Heslington, York, YO10 5DD, UK

(Dated: 18 February 2022)

Silk is a semi-dilute solution of randomly coiled associating polypeptide chains that crystallise following the stretch-induced disruption, in the strong extensional flow of extrusion, of the solvation shell around their amino acids. We propose that natural silk spinning exploits both the exponentially-broad stretch-distribution generated by associating polymers in extensional flow and the criterion of a critical concentration of sufficiently-stretched chains to nucleate flow-induced crystallisation. To investigate the specific-energy input needed to reach this criterion in start-up flow, we have coupled a model for the Brownian dynamics of a bead-spring-type chain, whose beads represent coarse-grained Gaussian chain segments, to the stochastic, strain-dependent binding and unbinding of their associations. We have interpreted the simulations with the aid of analytic calculations on simpler, tractable models with the same essential physical features. Our simulations indicate that the associations hamper chain alignment in the initial slow flow, but, on the other hand, facilitate chain stretching at low specific work at later, high rates. We identify a minimum in the critical specific work at a strain rate just above the stretch transition (i.e, where the mean stretch diverges), which we explain in terms of analytical solutions of a two-state master equation. We further discuss how the silkworm appears to exploit the chemical tunability of the associations to optimise chain alignment and stretching in different locations along the spinning duct: this delicate mechanism also highlights the potential biomimetic industrial benefits of chemically tunable processing of synthetic association polymers.

[a)]Electronic mail: charley.schaefer@york.ac.uk

PLEASE CITE THIS ARTICLE AS DOI: 10.1122/8.0000411

I. INTRODUCTION

The manufacturing of both natural and artificial polymer-based fibres relies on flow-induced crystallisation in non-linear rheological conditions[1–6]. The energy input required by this process may be significantly reduced in natural silk-spinning, though the mechanism by which this efficiency is achieved has been far from clear[7]. There is evidence, however, that locally-tailored macromolecular interactions are involved[8–11]: The silk protein, of which the conformation in solution closely resembles a random coil[12], self-assembles in flow in aqueous conditions under energy requirements orders of magnitude lower than its synthetic counterparts[7]. It has been hypothesised that flow-induced stretching of the chain disrupts a solvation layer and in turn enables crystallisation to commence[7,13,14]. This mechanism was supported by molecular dynamics simulations[15–18], and was employed to induce crystallisation of synthetic poly-ethylene oxide by flow at similarly low energetic requirements as silk, however, at much higher molecular weight and/or strain rates[13]. The low-energy mechanism for natural silk-spinning therefore remains to be identified. Clues may be present in the subtle electrostatically-modified rheo-physics of associating polymers[19–28].

We previously found, in collaboration with Laity and Holland, that the silk protein exhibits calcium bridges that act as intermolecular reversible cross-links[8,9]. Such associations, sometimes referred to as 'stickers' that can be in a bound/closed or unbound/open state[19], shift the alignment-to-stretch transition to smaller strain rates by replacing the usual Rouse relaxation dynamics for 'sticky Rouse' relaxation[19–28]. Inspired by these observations, we envision a mechanism of flow-induced crystallisation where the reversible network is initially equilibrated (in stark contrast to the typical mechanism for the sol-gel transition of associating polymers, where shear flow breaks metastable intramolecular associations, and facilitates the formation of an intermolecular network[29–31]). In our case, strong flow stretches the 'bridging' strands between the stickers[32,33]. This stretch in turn aligns the strands at the scale of the Kuhn segments (which in water-soluble systems may disrupt the solvation layer[7,13]), so nucleating crystals as structural elements within (silk) fibres. It will turn out that such a picture contains within it a mechanism for the super-efficiency of natural silk-spinning through a surprisingly strong heterogeneity in the chain stretch distribution.

While this mechanism seems plausible, it is not evident how this process may be controlled and/or optimised by the number of stickers per chain and by their lifetime. Intriguingly,

however, it has been observed that the *Bombyx mori* silkworm tunes the sticker lifetime, and hence the (non-)linear rheology, before and during spinning through local chemical control variables. Prior to pupation, i.e., when the silkworm is not required to spin a cocoon, the silk is stored in the gland at high viscosity using long sticker lifetimes[8,9]. When pupation commences, potassium cations are added to decrease of the sticker lifetime and reduce the viscosity[8,9].

We firstly hypothesise, as schematically indicated in Fig. 1, that the decrease of the sticker lifetime decreases the specific work needed to align the chains in the direction of the flow field well upstream from the spinnerette. The group of Holland also discovered that the structural features of the silk fibre are significantly enhanced through a gradient in the pH along the spinning duct, suggesting an exquisitely controlled local rheology[34]. While lower pH may induce partial folding of the protein[12], it is also expected to enhance the lifetime of the stickers. Crucially, inspired by our previous finding that broad conformational distributions emerge due to the stochastic nature of binding and unbinding stickers[10,11], we therefore hypothesise secondly that crystallisation may be initiated by reaching a critical concentration of highly stretched chain segments. This would require significantly less energy input than for stretching the entire population of chain segments.

To theoretically investigate this hypothesis, we focus our attention on the flow-induced preparation of the conditions for crystallisation (rather than crystallisation itself). We are in particular interested in the specific critical work

$$W(t_\mathrm{s}) = \int_0^{t_\mathrm{s}} \boldsymbol{\sigma} : \boldsymbol{\kappa} \mathrm{d}t, \tag{1}$$

required to induce flow-induced crystallisation after a period time t_s during which the system is subjected to the (experimentally controllable) transpose of the (local) velocity-gradient tensor $\boldsymbol{\kappa} = \boldsymbol{\nabla}\mathbf{v}^\mathrm{T}$, and the (local) stress response $\boldsymbol{\sigma}$. The integral is taken in the (local) Lagrangian co-moving frame of a fluid element. In experimental works (see Ref. 35–37 and citations therein), the shear rate and duration t_s render the specific work a control variable ($W \approx \sigma_{xy}\dot{\gamma}t_\mathrm{s}$) that controls the number of nuclei generated in the system. As the efficiency to converse the energy input into nucleation events is rather limited (estimated $\approx 1\%$[37]), it is worth investigating how the energy loss may be reduced, e.g., by making use of intermolecular associations.

Clearly, the formation of nuclei must be controlled by the underlying molecular con-

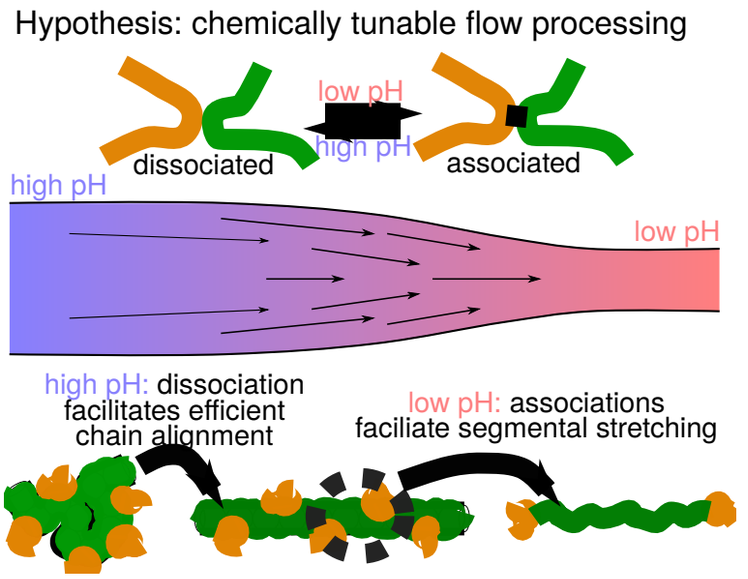
Hypothesis: chemically tunable flow processing
low pH
high pH
dissociated
associated
high pH
low pH
high pH: dissociation
facilitates efficient
chain alignment
low pH: associations
faciliate segmental stretching

potentials. At this level of computational detail, sticker dissociation may occur following attempts to escape the attractive potential through molecular vibrations[46,47]. These MD simulations are, however, computationally very demanding, as the dissociation events are quite rare. However, because of this rarity of events, the local equilibration of the chains enables a much simpler description of the chain dynamics in terms of the fraction of closed stickers, p and their lifetime, τ_s[19]: In a coarse-grained picture, this sticker lifetime is an elementary rather than an emergent timescale. This allows a description of the problem in terms of the dynamics of a single chain in a crowded environment[10,11,48–50], an approach similar to the modelling of entangled polymers through slip-link and slip-spring models[45,48,51–56], where the generation and destruction of entanglements are modelled as elementary processes.

While there is no unique way of formulating a coarse-grained single-chain model[57], all variants of bead-spring, slip-link and slip-spring models can be written in the general form

$$\zeta_i \frac{\partial \mathbf{R}_i}{\partial t} = \mathbf{F}_{\text{intra},i} + \mathbf{F}_{\text{thermal},i} + \mathbf{F}_{\text{flow},i} + \mathbf{F}_{\text{network},i}, \tag{2}$$

where i is a chain segment at position $\mathbf{R}_i$ that is thermally equilibrated at the relevant time scales[58]. We will refer to this chain segment as a 'node' of an elastic network, which may represent a non-sticky segment of a chain (a purely frictional 'bead'), a segment with a reversible association (a 'sticker'), or it may be an entangled segment (a 'slip-link' or a 'slip-spring'). Which of these representations is invoked manifests itself in the definition of the friction coefficient, ζ_i, the (friction-dependent) thermal forces, $\mathbf{F}_{\text{thermal},i}$, and the network forces, $\mathbf{F}_{\text{network},i}$. For instance, in classes of models where nodes move affinely with the flow field, the network force exactly cancels the sum of the (conformation-dependent) intramolecular force and the thermal force, $\mathbf{F}_{\text{network},i} = -\mathbf{F}_{\text{intra},i} - \mathbf{F}_{\text{thermal},i}$. This 'rigid-network approximation' is tacitly invoked in the slip-link model by Hua and Schieber[54] and in our recently published model for sticky-polymers in a rigid network[10,11]. Within Likhtman's slip-spring model, the slip-spring may diffuse within a potential energy landscape that represents the elastic compliance of the entangled network[55]. In the present work, we will account for the compliance experienced by the stickers in a reversible network.

In the following, in Section II A we present the usual intramolecular, thermal and drag forces that act on single chains. To capture how the stickers modify the intermolecular forces (i.e., the 'elastic compliance' of the surrounding network) and the segmental drag, we present a non-spatially-explicit multi-chain approach. In Section II B, we present a

two-state master equation that generates analytical predictions of the impact of sticker opening and closing on both the steady-state and transient stretch distributions of the chains, which enables us to interpret our simulated data in Section III. By first mapping the results in the linear flow regime to the analytic sticky-reptation (SR) model, in Section III A we discuss how the stochastic nature of sticker opening and closing and the elastic compliance affects the linear rheological data. Then, in Section III B we show how a broad steady-state distribution of chain conformations emerges in strongly non-linear flows of shear and extension. By simulating the transient emergence of these distributions in start-up flow in Section III C, we show that the stickers initially hamper the collective alignments of the chains in mildly non-linear aligning flows, but facilitates the emergence of stretched outliers. In Section III D we discuss how these outliers may reduce the critical specific work for flow-induced crystallisation. In the discussion and conclusions of Section IV we use our findings to interpret the experimental observations of silk spinning, and argue that the chemical tuning of associations is indeed a promising mechanism to control the flow-induced crystallisation of artificial materials.

II. MODEL AND THEORY

A. Brownian dynamics of Sticky Polymers in Flow

In this section we will present a coarse-grained description of associating polymers, where the dynamics of sticker opening and closing will depend on the number of open and closed stickers in a non-spatially-explicit collection of chains. Any linear polymer that consists of N monomers may be discretised using a number of nodes, N_{nodes}, see Fig. 2. We use the wording 'node' to emphasise that the node may not just represent a traditional, frictional bead of a bead-spring model, but may also represent a sticker that can be in an open or closed state, or a slip-link or slip-spring (which, unlike traditional beads, may fluctuate in numbers). Each node i is located at a spatial coordinate $\mathbf{R}_i$ relative to the centre of mass of the chain. The strand between neighbouring nodes i and $i+1$ has an end-to-end vector $\mathbf{Q} = \mathbf{R}_{i+1} - \mathbf{R}_i$ and contains a fraction $\Delta s_i = N_{\text{s},i}/(N+1)$ of all the monomers in the chain.

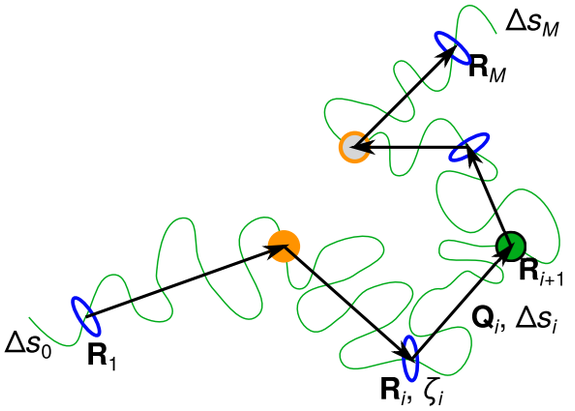

FIG. 2. The theory in Section II A applies to sticky entangled poymers that are parameterised using the locations of M nodes. Each node may be a bead (green disk), a sliplink/entanglement (blue ellipses), a closed sticker (orange disk), or an open sticker (orange circles). All nodes are assigned a friction ζ_i that depends on the fraction of monomers of the chain, Δs_i, that reside in each of the $M+1$ substrands, see Eq. (3). In general, the number of beads and entanglements may fluctuate during a simulation. In the present work, we focus on the physics of the stickers and fix the number of beads and do not include any entanglements.

At this level of coarse-graining, the friction of each node is given by

$$\zeta_i = N\zeta_0 \begin{cases} \Delta s_{i-1} + \Delta s_i/2, & \text{for } i = 1 \\ (\Delta s_{i-1} + \Delta s_i)/2, & \text{for } 1 < i < N_{\text{nodes}} \\ \Delta s_{i-1}/2 + \Delta s_i, & \text{for } i = N_{\text{nodes}} \end{cases}, \tag{3}$$

with ζ_0 the monomeric friction. The assumption that the dangling chain ends are relaxed may be released by explicitly modelling the position of the chain ends and setting $\Delta s_i \equiv 0$ at $i = 0$ and at $i = N_{\text{nodes}}$[59].

The equilibrium structure of the chain in quiescent conditions is determined by the end-to-end distance of the substrands, $|Q_i| = \lambda b(\Delta s_i N)^{1/2}$, where the stretch ratio λ obeys the equilibrium distribution

$$P(\lambda) = 4\pi\lambda^2 \left(2\pi/3\right)^{-3/2} \exp\left(-\frac{3\lambda^2}{2}\right). \tag{4}$$

This distribution emerges as a consequence of the intramolecular and thermal forces in Eq. (2).

In order to derive the intramolecular spring forces, we consider the spring force of the entire chain of N monomers with a mean stretch ratio of unity

$$F_{\text{intra}}^{\text{strand}} = \frac{3k_{\text{B}}T}{bN^{1/2}} k_{\text{s}}(\lambda;\lambda_{\max})(1-\lambda), \tag{5}$$

where

$$k_{\text{s}}(\lambda;\lambda_{\max}) = \frac{(3\lambda_{\max}^2-\lambda^2)/(\lambda_{\max}^2-\lambda^2)}{(3\lambda_{\max}^2-1)/(\lambda_{\max}^2-1)}. \tag{6}$$

approximately captures the anharmonicity of the spring force due to the finite extensibility of the substrand[60]. For the substrands i the harmonic spring force is larger than that of the full chain, and the maximum stretch ratio is smaller. This is captured by the renormalisation $F_{\text{intra}} \mapsto F_{\text{intra},i}$, $N \mapsto \Delta s_i N$, and $\lambda_{\max} \mapsto \Delta s_i^{1/2}\lambda_{\max} \equiv \lambda_{\max,i}$. The direction of the force exerted by spring i on node i is $\mathbf{Q}_i/|\mathbf{Q}_i|$, while the direction of this force acted upon node $i+1$ is $-\mathbf{Q}_i/|\mathbf{Q}_i|$. Hence, the net intramolecular force exerted on node i is

$$\mathbf{F}_{\text{intra},i} = F_{\text{intra},i-1}^{\text{strand}} \frac{\mathbf{Q}_{i-1}}{|\mathbf{Q}_{i-1}|} - F_{\text{intra},i}^{\text{strand}} \frac{\mathbf{Q}_i}{|\mathbf{Q}_i|} \tag{7}$$

The thermal force is given by the equipartition theorem

$$\langle \mathbf{F}_{\text{thermal},i}(t)\rangle = \mathbf{0}; \tag{8}$$

$$\langle \mathbf{F}_{\text{thermal},i,\alpha}(t)\mathbf{F}_{\text{thermal},i,\beta}(t')\rangle = 0, \text{ for } \alpha \neq \beta \tag{9}$$

$$\langle \mathbf{F}_{\text{thermal},i,\alpha}(t)\mathbf{F}_{\text{thermal},i,\beta}(t')\rangle = 2k_{\text{B}}T\zeta_i\delta(i'-i)\delta(t'-t), \text{ for } \alpha = \beta \tag{10}$$

with $\alpha,\beta = x,y,z$ the Cartesian coordinates and $k_{\text{B}}T$ the thermal energy.

The force acted upon the nodes by flow is, provided that our coordinate system moves with the flow field, given by

$$\mathbf{F}_{\text{flow},i} \equiv \zeta_i \left.\frac{\partial \mathbf{R}_i}{\partial t}\right|_{\text{flow}} = \zeta_i \boldsymbol{\kappa}\cdot\mathbf{R}_i, \tag{11}$$

where $\boldsymbol{\kappa}$ is the transpose of the velocity-gradient tensor, which in extension and shear is given by

$$\boldsymbol{\kappa} = \frac{1}{2}\begin{pmatrix} 2\dot{\varepsilon} & 0 & 0 \\ 0 & -\dot{\varepsilon} & 0 \\ 0 & 0 & -\dot{\varepsilon} \end{pmatrix}, \text{ and } \boldsymbol{\kappa} = \begin{pmatrix} 0 & \dot{\gamma} & 0 \\ 0 & 0 & 0 \\ 0 & 0 & 0 \end{pmatrix}, \tag{12}$$

respectively. As the coordinate system moves with the flow field, the spatial quantities of physical interest to calculate are the deformation of the individual substrands

$$\left.\frac{\partial \mathbf{Q}_i}{\partial t}\right|_{\text{flow}} = \boldsymbol{\kappa}\cdot\mathbf{Q}_i, \tag{13}$$

PLEASE CITE THIS ARTICLE AS DOI: 10.1122/8.0000411

using which we recursively obtain the drift of the nodes as

$$\left.\frac{\partial \mathbf{R}_{i+1}}{\partial t}\right|_{\text{flow}} = \left.\frac{\partial \mathbf{Q}_i}{\partial t}\right|_{\text{flow}} + \left.\frac{\partial \mathbf{R}_i}{\partial t}\right|_{\text{flow}}. \tag{14}$$

The value of the first entry, $\partial \mathbf{R}_1/\partial t$ is adjusted to fix the centre of mass of the chain (this assumes that the centre of mass moves affinely with the flow field).

The dynamics of the chain conformation depends on the state of the stickers through the network force, which in turn depends on the dynamics of sticker opening and closing and so, finally, on the chain conformation itself. In particular, when chain segments are highly stretched, the network forces may cause the stickers to dissociate. To obtain these forces we simulate multiple chains and track the collection of open and closed stickers. When sticker i from chain A and sticker j from chain B are closed to form a pair, the friction coefficient, the thermal force, and the network force are modified until the sticker pair opens again. The friction coefficient of both nodes becomes $\zeta_i^{\mathrm{A}} + \zeta_j^{\mathrm{B}}$, where ζ_i^{A} and ζ_j^{B} are given by Eq. (3), and the thermal forces are given by the equipartition theorem Eq. (10) as before, but with this modified friction coefficient. The network forces are now given by

$$\mathbf{F}^{\mathrm{A}}_{\text{network,i}} = \mathbf{F}^{\mathrm{B}}_{\text{intra,j}}, \text{ and by } \mathbf{F}^{\mathrm{B}}_{\text{network,j}} = \mathbf{F}^{\mathrm{A}}_{\text{intra,i}}. \tag{15}$$

Hence, the paired stickers i and j have an identical friction coefficient and experience the same net force $\mathbf{F}^{\mathrm{A}}_{\text{intra,i}} + \mathbf{F}^{\mathrm{B}}_{\text{intra,j}} + \mathbf{F}^{\mathrm{A}}_{\text{thermal,i}}$ (where $\mathbf{F}^{\mathrm{A}}_{\text{thermal,i}} = \mathbf{F}^{\mathrm{B}}_{\text{thermal,j}}$). Crucially to forced sticker dissociation, the net force that acts on the closed sticker pair is

$$F_{\text{stic}} = |\mathbf{F}^{\mathrm{A}}_{\text{intra,i}} - \mathbf{F}^{\mathrm{B}}_{\text{intra,j}}|, \tag{16}$$

which we assume, as in other cases of forces temporary unbinding, lowers the activation energy for sticker dissociation as

$$E_{\text{act}} = E^0_{\text{act}} - \ell F_{\text{stic}} \tag{17}$$

with E^0_{act} the activation energy in quiescent conditions and ℓ the typical length scale associated with sticker dissociation[11]. We remark that the (apparent) activation energy obtained from experiments using the Arrhenius-type equation[24] $\tau_{\text{s}} = \nu^{-1} \exp(E_{\text{act}}/k_{\text{B}}T)$, for the sticker lifetime with ν an attempt frequency, may be much larger than this activation energy for dissociation. This is due to fast sticker recombination processes[9,61] or due to the mixing of various mechanisms of sticker opening and closing, such as bondswapping[11,62].

For now, we assume a well-defined pairwise association-dissociation reaction whose equilibrium condition is described by the detailed balance $p/(1-p)^2 = K_0 \exp(-\ell_0 F_{\text{stic}})$, with K_0 the equilibrium constant in the absence of any chain tension. Here, the free energy $\ell_0 F_{\text{stic}} > 0$ captures the shift in detailed balance (i.e., the fraction of closed stickers decreases with an increasing chain tension), while ℓF_{stic} in Eq. (17) modifies the rate by which the equilibrium is reached. Indeed, in terms of transition state theory, we may write the opening and closing rates as $k_{\text{open}} = \nu \exp([\theta \ell_0 F_{\text{stic}} - E^0_{\text{act}}]/k_{\text{B}}T)$ and $k_{\text{close}} = \nu K_0 \exp(-[(1-\theta)\ell_0 F_{\text{stic}} + E^0_{\text{act}}]/k_{\text{B}}T)$, respectively, where $\ell \equiv \theta \ell_0$, and where $\theta \in [0, 1]$ is the so-called Brønsted-Evans-Polanyi coefficient[63]. While its value may be determined using experiments or atomistic simulations, we know that θ must be larger than zero in order to capture strain-induced sticker dissociation[29–33]. We argue that the rheological physics of a reversible polymer network does not necessitate exact knowledge of θ: When a sticker opens, it may freely diffuse and find conditions to bind to another sticker that is not subject to the influence of strongly stretched chain segments: association will typically take place in conditions where the activation barrier is equal to that in quiescent conditions. Indeed, in our simulations we find that the mean fraction of open stickers in conditions of strong flow remains similar to the fraction in quiescent conditions, despite noticable acceleration of sticker dissociation.

These arguments have enabled us to conveniently set $\ell = \ell_0$ and $\theta = 1$; the latter avoids the need for on-the-fly calculations of association rates during our simulation. We have implemented the opening and closing of stickers using a kinetic Monte Carlo (kMC; also known as a Discrete Event Simulation) scheme, where after a time interval Δt a sticker is opened or closed with a probability $(1 - \exp[-k_{\text{open}}\Delta t])$ or $(1 - \exp[-k_{\text{close}}\Delta t])$, respectively. In our simulation algorithm, shown in Fig. 3 and discussed in detail in Appendix V A, we take time steps during which the chain conformations are approximately fixed, and for which the time-independent (but conformation-dependent) rates of sticker opening and closing are calculated. The dynamics of the stickers is simulated during the time step using a kMC scheme. This essentially creates and destroys constraints in a similar way as in the slip-link model[54], but where the constraints physically represent closed stickers instead of entanglements (hence, our approach may be generalised using appropriate kMC algorithms[64–66] to go beyond the unentangled chains with pairwise association and dissociation of stickers focussed on in the present work, and also capture entanglements, stickers that dimerise through bondswapping, and stickers that may assemble into larger aggregates). After this step of

'constraint-dynamics' the Brownian dynamics are solved, the conformations are updated, and the next time step is commenced.

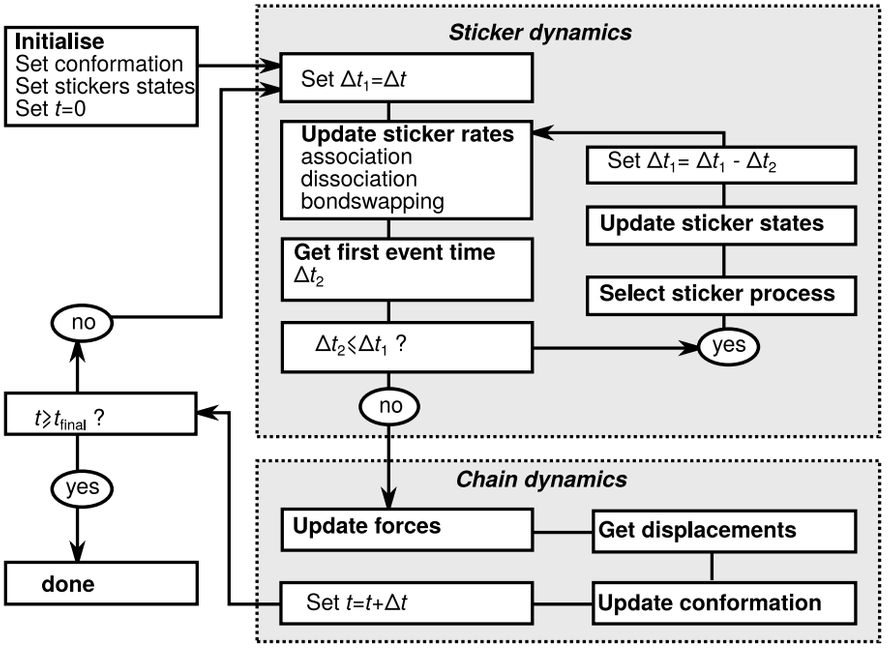

FIG. 3. Flow chart of the algorithm to simulate the conformational dynamics of sticky polymers and the dynamics of sticker association and dissociation (detailed discussion: see Appendix V A).

B. Approximate theory in transient extensional flow: Two-state model

The dynamics of sticky polymers is complicated by the fact that a polymer with Z_s stickers can be in 2^{Z_s} different states, as each individual sticker can be either open or closed. An instructive simple case is a chain with $Z_s = 2$, as the chain is either completely free to relax when either of the stickers is open (state 1), or can only be extended by flow when both stickers are closed (state 0). Hence, we can accurately distinguish between an extension state where the polymer is unable to relax and a relaxation state where the polymer is able to relax. Using this 'two-state' description, we previously discovered that stickers give rise to enormous stretch fluctuations in extensional flow below the strain rate at which the mean stretch diverges, i.e., below the 'stretch transition', which are descibed by the steady-state power-law stretching distribution[10]

$$P(\lambda) \propto \lambda^{\nu}, \text{ with } \nu < 1, \text{ and for } \lambda \gg 1. \tag{18}$$

It turned out that this two-state prediction, which is exact for chains with two stickers, also described the steady-state stretch distribution for chains with multiple stickers. In the present work, we recapitulate our previous analysis of the steady-state situation and extend it for transient start-up flow. In all of this analysis we will consider a single relaxation mode of the polymer at time scales beyond the relaxation time of the surrounding network; hence, we invoke the rigid-network approximation in this entire section.

The starting point is to consider a chain in two states where the chain is either unable to retract (state 0) or is free to retract (state 1). The opening rate is k_{open} and the closing rate is k_{close}. The time development of the probability distribution of the stretch ratio is described by[10]

$$\frac{\partial P_0}{\partial t} = -\frac{\partial}{\partial \lambda}\left[\dot{\varepsilon}\lambda P_0\right] \qquad -k_{\text{open}}P_0 + k_{\text{close}}P_1, \tag{19}$$

$$\frac{\partial P_1}{\partial t} = -\frac{\partial}{\partial \lambda}\left[\left(\dot{\varepsilon}\lambda + \frac{1-\lambda}{\tau_{\text{R}}}\right)P_1\right] + k_{\text{open}}P_0 - k_{\text{close}}P_1, \tag{20}$$

with τ_{R} the bare Rouse time of the chain without stickers. In this equation, we have neglected the high-frequency relaxation modes of the polymer, as well as the (potentially much slower) relaxation of the surrounding network; the latter is justified in view that the network rapidly stiffens with an increasing strain. To approximate this equation analytically, we first make the substitution $y \equiv \ln\lambda$, so $\partial P_i/\partial\lambda = (1/\lambda)\partial P_i/\partial \ln\lambda \equiv \exp(-y)\partial P_i/\partial y$. Similarly, $\partial\lambda P_i/\partial\lambda = P_i + \partial P_i/\partial y$. Inserting this into the governing equations gives

$$\frac{\partial P_0}{\partial t} = -\dot{\varepsilon}\frac{\partial P_0}{\partial y} \qquad -\left(\dot{\varepsilon} + k_{\text{open}}\right)P_0 + k_{\text{close}}P_1, \tag{21}$$

$$\frac{\partial P_1}{\partial t} = -\left(\dot{\varepsilon} + \mathrm{e}^{-y} - \tau_{\text{R}}^{-1}\right)\frac{\partial P_0}{\partial y} \qquad +k_{\text{open}}P_0 - \left(k_{\text{close}} + \dot{\varepsilon} + \mathrm{e}^{-y} - \tau_{\text{R}}^{-1}\right)P_1. \tag{22}$$

The non-linear contributions can then be omitted by considering the limit of large stretches where their contribution to the distribution is exponentially small, i.e., we approximate $\mathrm{e}^{-y} \approx 0$, which is equivalent to $\lambda \gg 1$.

In steady state, the left-hand side of the equation is zero and the equations can be cast in the form $\mathrm{d}\mathbf{P}/\mathrm{d}y = \mathbf{A}\cdot\mathbf{P}$, with $\mathbf{P} = [P_0,\, P_1]^{\text{T}}$ and $\mathbf{A}$ a constant 2 by 2 matrix. The solution of this system of first-ordinary differential equations is given by[10]

$$P_0^{\text{eq}} = c\lambda^{\nu}, \tag{23}$$

$$P_1^{\text{eq}} = \frac{k_{\text{close}}}{k_{\text{open}}}\frac{\dot{\varepsilon}}{\left(\dot{\varepsilon} - \tau_{\text{R}}^{-1}\right)}P_0^{\text{eq}}, \tag{24}$$

with c a normalisation constant (its value can in principle be determined by releasing the approximation $\mathrm{e}^{-y} \approx 0$), and with the exponent of the power-law distribution given in terms of physical parameters by

$$\nu = -1 + \frac{k_{\mathrm{close}}}{(\tau_{\mathrm{R}}^{-1} - \dot{\varepsilon})} - \frac{k_{\mathrm{open}}}{\dot{\varepsilon}} = -1 + \frac{1}{(1 - \dot{\varepsilon}\tau_{\mathrm{R}})} \frac{p}{(1-p)} \frac{\tau_{\mathrm{R}}}{\tau_{\mathrm{s}}} - \frac{1}{\dot{\varepsilon}\tau_{\mathrm{s}}}. \tag{25}$$

(this is one of the eigenvalues of Eq. (21) and Eq. (22); the other eigenvalue is -1 and is unphysical as a distribution of the form λ^{-1} cannot be normalised.) The value of this stretching exponent diverges if the bare stretch transition at $\dot{\varepsilon}\tau_{\mathrm{R}} = 1$ is approached from small strain rates. However, because of the physics of the stickers, actual divergence already occurs at lower strain rates: At $\dot{\varepsilon}\tau_{\mathrm{R}} = (1-p)$, the exponent becomes $\nu = -1$ and the stretch distribution can no longer be normalised. Depending on the sticker lifetime, at smaller strain rates the exponent may reach a value $\nu = -2$ if the 'sticky Weissenberg number' $(1-p)\dot{\varepsilon}\tau_{\mathrm{R}}$ reaches unity; here, the mean stretch diverges. While the mean stretch is finite for smaller strain rates, the variance of the stretch diverges for $\nu \geq -3$, which happens if $(1-p)\dot{\varepsilon}\tau_{\mathrm{R}}$ becomes larger than $1/2^{10}$, at which point (considerably slower than the bare stretch transition) we expect a long tail of very high stretched chains to develop in the distribution.

This analytic approach can be extended to predict the transient dynamics of the distribution in start-up flow. As we will show, the late-stage dynamics in which the tail of the distribution 'fills up' is independent of the initial conditions. In those late stages, the distribution reaches a steady state for stretches below a certain 'front', $\lambda_*(t)$ (above which the distribution function has a value of zero) which shifts to high stretch values over time. The precise number of chains with a certain stretch also depends on the width of this moving front. We assess analytical predictions on the front position and width using the two-state model using solutions in an early- and late-stage regime, where the time scale is, respectively, much shorter and much larger than the sticker lifetime. While the long-time regime will slow down the progression of the front due to sticker opening, in the early-stage regime we will obtain an upper limit of the rate by which the front moves.

In the early-stage regime, we approximate the stretch distribution using a the Dirac-delta distribution (justified by the very wide long-time distribution), $P_i(t=0,\lambda) = c_i\delta(\lambda - \lambda_*(0))$ at $\lambda_*(0)$, from which it can be easily seen that the distributions shift initially, when pure advection dominates over sticker dynamics, to higher stretches for the closed state, $P_0(t,\lambda) =$

$c_0\delta(\lambda - \lambda_*(0)\exp[\dot{\varepsilon}t])$ and retract to smaller stretches for the open state $P_1(t,\lambda) = c_1\delta(\lambda - \lambda_*(0)\exp[-(\tau_{\mathrm{R}}^{-1} - \dot{\varepsilon})t])$. This suggests that the 'front', $\lambda_*(t)$, of any distribution with finite P_0, shifts exponentially in time to higher values through $\lambda_*(t) = \lambda_*(0)\exp[\dot{\varepsilon}t]$.

To develop an analytic approximation for the long-time limiting behaviour of the sticky polymers in start-up flow, we consider some point in time $t_0 \gg \tau_{\mathrm{SR}}$ where sufficient stickers have opened to facilitate chain relaxation, and assume that the stretch distribution has reached a steady-state for small stretches $\lambda < \lambda_*(t_0)$, but is empty for larger stretch ratios. Here, $\lambda_*(t_0)$ can be thought of as the establishment of the 'front' of the stretch distribution at later times moving to higher stretches. In the following, we will show that the ansatz of this moving front is indeed a good approximation for the tail of the transient stretch distribution and that for later times $t > t_0$, further convergence of the stretch distribution takes place in the range of stretches $\lambda_*(t_0) < \lambda < \lambda_*(t)$, where the 'front' of the distribution shifts to high stretch values as $\ln[\lambda_*(t)/\lambda_*(t_0)] \propto \dot{\varepsilon}(t - t_0)$. Assuming that $\lambda_*(t_0) \gg 1$, the steady-state portion of the distribution is negligibly affected by the loss of small-stretch contributions to the tail of the distribution (see discussion around Eq. (51) in Appendix V B), and for any time $t' > t_0$ the $\lambda < \lambda_*(t')$ portion of the stretch distribution becomes independent of time beyond $t > t'$. The constancy of the distribution at $\lambda_*(t_0)$ provides a fixed-boundary condition. Hence, this problem essentially models the dynamical response to a unit step, and lends itself to an analysis through a Laplace transform to give a solution for the distribution at each stretch ratio λ of the form $\exp(-s\tau(\lambda))/s$, which is the Laplace transform of a time-dependent function that becomes non-zero at the time $\tau(\lambda)$. The inverse function $\lambda(\tau)$ is then the trajectory of the 'front' of the distribution. In Appendix V B, we detail the Laplace transform of Eqs. (21-22) with the boundary condition in this long-time regime, which as a solution gives

$$P_0(t,\lambda_*(t)) = c\left(\frac{\lambda_*(t)}{\lambda_*(t_0)}\right)^{\nu}\Theta(\nu'\ln[\lambda_*(t)/\lambda_*(t_0)] - \dot{\varepsilon}t) \tag{26}$$

$$P_1(t,\lambda_*(t)) = \frac{k_{\mathrm{close}}}{k_{\mathrm{open}}}\frac{\dot{\varepsilon}}{(\dot{\varepsilon} - \tau_{\mathrm{R}}^{-1})}P_0(t,\lambda), \tag{27}$$

with ν the 'steady-state stretch exponent' in Eq. (25) and with

$$\nu' = \left(1 - \frac{1}{1-\mathrm{Wi}} + \frac{1}{1-\mathrm{Wi}^{\mathrm{sticky}}}\right) \tag{28}$$

the 'dynamic stretch exponent', which controls the growth of the front of the distribution

as

$$\lambda_*(t) = \lambda_*(t_0) \exp\left(\frac{\dot{\varepsilon}(t-t_0)}{\nu'}\right). \tag{29}$$

In this equation, $\mathrm{Wi} = \dot{\varepsilon}\tau_\mathrm{R}$ and $\mathrm{Wi}^\mathrm{sticky} = \dot{\varepsilon}\tau_\mathrm{SR}$ are the (extensional) Weissenberg numbers of the chain without and with stickers, respectively; within the two-state model, $\tau_\mathrm{SR} = (1-p)/k_\mathrm{open}$, see discussion under Eq. (25). Upon approaching the stretch transition $\mathrm{Wi}^\mathrm{sticky} = 1$ where the mean stretch diverges, $\nu' \approx 0$ indicates 'critical slowing down', as the (late-stage) front of the distribution becomes immobile. For chains with strong stickers $(1-p)\tau_\mathrm{s} \gg \tau_\mathrm{R}$ at the strain rate $\mathrm{Wi}^\mathrm{sticky} = 1/2$ where the variance of the stretch diverges (see discussion under Eq. (25)), we find $\nu' \approx 2$, which indicates that the late-stage measure of the front is shifted from the early-stage measure for the outliers by a factor 2. We have also checked that the moving front is narrow for small strain rates $\mathrm{Wi}^\mathrm{sticky} < 1/2$. In Appendix V B, we provide more analytical analysis of the two-state model to estimate the width of the front (relative to its extent) as $\Delta_\mathrm{rel} \propto \sqrt{p\mathrm{Wi}\mathrm{Wi}^\mathrm{sticky}/(1-\mathrm{Wi}^\mathrm{sticky})}$, where $\Delta_\mathrm{rel} \approx \left(\partial[P(\lambda,t)/P_\mathrm{eq}(\lambda,\infty)]/\partial \ln\lambda\right)^{-1} / \ln\lambda$. As we show in Appendix V B, typically this width is $\Delta_\mathrm{rel} \ll 1$, and the front of the distribution is narrow even close to the stretch transition.

III. RESULTS

A. Linear dynamics

We have verified the physics of our model in the linear viscoelastic regime by first simulating non-sticky chains of fixed length but a varying number of beads from $M = 4$ to 64 (the beads are regularly along the backbone of the polymer, so $\Delta s_i = 1/(M+1)$ for all i). Fig. 4 shows that the choice of the number of beads has a negligible influence on the time evolution of the mean-square displacement, MSD, of the centre of mass and is in all cases in agreement with the theoretical prediction

$$\mathrm{MSD} = 6Dt, \tag{30}$$

where the diffusivity, D, is for non-sticky polymers given by the bare Rouse diffusivity

$$D_\mathrm{R} = \frac{1}{3\pi^2}\frac{\langle R_\mathrm{e}\rangle^2}{\tau_\mathrm{R}}. \tag{31}$$

Moreover, the inset of Fig. 4 shows that also the end-to-end-distance, R_e, is distributed according to the physical equilibrium result of Eq. (4).

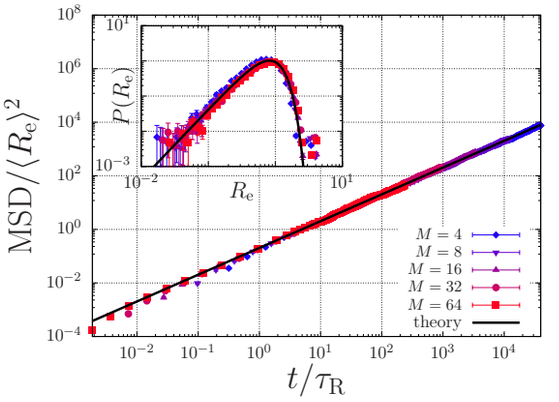

FIG. 4. Mean-square displacement, MSD, of the centre of mass of a non-sticky polymer against time (main panel) and the time-averaged end-to-end length (R_e) distribution (inset). The number of real monomers per chain is fixed, while the level of coarse-graining is varied through varying the number of beads, M, per chain. The symbols and solid black curves represent the simulations and the theory, respectively.

For times shorter than the Rouse time of strands between stickers, i.e., for $t < \tau_\mathrm{R}(Z_\mathrm{s}{+}1)^{-2}$, the dynamics of a sticky polymer are governed by the same Rouse diffusion as non-sticky chains, see Fig. 5(a). For later times than that, the motion of the polymer is subdiffusive until the sticky Rouse time τ_SR, which is approximately given by[19]

$$\tau_\mathrm{SR} = \tau_\mathrm{s} Z_\mathrm{s}^2 \left(1 - \frac{9}{p} + \frac{12}{p^2}\right)^{-1}. \tag{32}$$

Focussing on the crossover from early-stage bare Rouse diffusion to subdiffusive motion, one would expect this crossover to occur at the point in time where the substrands between stickers have just relaxed, and where further relaxation requires sticker dissociation. Indeed, we find this is the case within the rigid-network approximation. However, for the elastically compliant network the closed stickers themselves are able to diffuse. The friction experienced by the closed sticker depends on the level of deformation of the surrounding network, which is initially small. As the sticker diffuses further, a larger portion of the surrounding network is deformed and the contribution of 'next-neighbour' stickers starts to contribute to the friction. Clearly, the increase of the friction increases rapidly beyond a certain characteristic

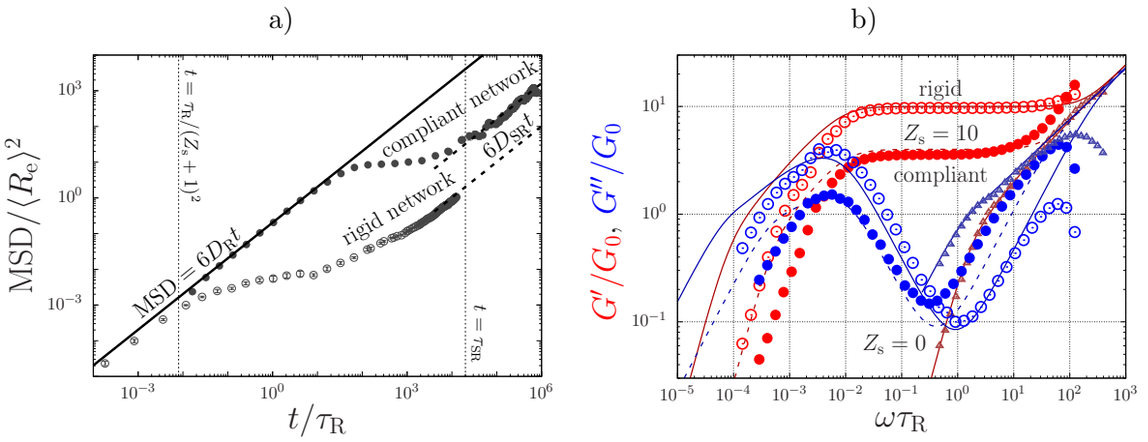

FIG. 5. Linear rheology of a sticky chain with $Z_s = 10$, $p = 0.9$, $\tau_s = 200\tau_R$ within the rigid-network approximation (open symbols) and with this approximation released (closed symbols). (a) Mean-square displacement MSD of the centre of mass against time. (b) Storage, G', and loss, G'', modulus in units of G_0 against the frequency, ω, plotted for the chain in (a) as well as for an non-sticky chain (triangles). There is fair agreement with the analytical sticky-Rouse model in Eq. (33) (solid curves) for the sticky chain within the rigid-network approximaton an for the non-sticky chain. For the sticky chain with an elastically compliant network the plateau modulus decreases to that of the theory with $Z_s = 4$ (dashed curves).

distance. It is unknown what this distance might be, but it is likely to be strongly dependent on the topology of the network. The plateau value in Fig. 5(a) shows that for our simulations this happens to occur when the MSD of the centre of mass of chain is approximately 10, i.e., when the centre of mass of the chain has diffused $3-4$ times its end-to-end distance.

The elastic compliance not only affects the subdiffusive motion of the chain, but also the sticky Rouse diffusivity $D_{SR} = D_R\tau_R/\tau_{SR}$ at times beyond the sticky Rouse time. While the analytical expression for the sticky Rouse diffusivity accurately describes our simulations within the rigid-network approximation, we find that it overestimates the diffusivity of chains in an elastically compliant network. We have investigated the consequence of this to the interpretation of linear viscoelastic data, which are often used experimentally to estimate the number of associations per chain, by calculating the dynamic moduli G' and G'' against the frequency ω in Fig. 5(b). The data shown includes non-associating unentangled chains ($Z_s = 0$) and the unentangled sticky chains of Fig. 5(a); i.e., chains with $Z_s = 10$ stickers within the rigid-network approximation and with an elastically compliant network. The

PLEASE CITE THIS ARTICLE AS DOI: 10.1122/8.0000411

simulated data (symbols) were obtained from the relaxation modulus, $G(t)$, through the multiple-tau-correlator algorithm discussed in Ref.[67]. To obtain the dynamic moduli G' amd G'' we have used the finite-element approach from Ref.[68]. We have compared the data to the sticky-Rouse model (curves), which is given by

$$G(t) = G_0 \sum_{p=Z_s+1}^{N} \exp\left(-\frac{2p^2 t}{\tau_R}\right) + G_0 \sum_{p=1}^{Z_s} \exp\left(-\frac{2p^2 t}{\tau_s Z_s^2}\right). \tag{33}$$

In this equation, the first summation captures the high-frequency bare Rouse modes (the number of Kuhn segments, N, truncates the highest frequencies), and the second summation captures the sticky Rouse modes. The modulus G_0 is proportional to the number density of monomers and to the thermal energy.

Fig. 5(b) shows dominance of bare Rouse relaxation at high frequencies, where all moduli will approach (in principle) the scaling relation $G', G'' \propto \omega^{1/2}$. Discrepancies, such as a roll-off of G'' at high frequencies, emerge due to the finite number of modes/beads that are included in the simulations. At decreasing frequencies the moduli of the non-sticky chains (triangles) decrease rapidly, while the moduli of the sticky chains reach a plateau value that ranges down to $\omega = 1/\tau_s$. Within the rigid-network approximation (closed circles), the modulus of the plateau is $G'(\omega) = G_0 Z_s$ in agreement with the sticky-Rouse model in Eq. (33) for $Z_s = 10$. However, if the network is elastically compliant (open circles), the plateau value decreases and is better described if the theory would be adjusted with an apparent number of stickers $Z_s = 4$ (dashed curves). At lower frequencies $\omega < 1/\tau_s$ the moduli rapidly decrease. In the simulations the moduli decrease much more rapidly than in the theory, as also noted earlier in Ref. 50. We find that this terminal relaxation time (we remind the reader that this relaxation time is for unentangled chains entirely determined by sticker relaxation, i.e., not by sticky reptation[22,24]) is even further reduced for the chain in an elastically compliant network. Consequently, the peak of the dynamic modulus G'' is much narrower than in the theory. We have estimated that the shape of this peak is best described by $Z_s = 4$ within the rigid-network approximation and $Z_s = 3$ for the compliant network. This clearly indicates that analysis of the dynamic modulus peak in rheological data (which is required when high frequencies are experimentally inaccessible[9]) provides an underestimate of the actual number of stickers per chain.

To obtain a wider view of the impact of the elastic compliance on the dynamics of chains with a various number of stickers and sticker lifetimes, we have calculated the diffusivities

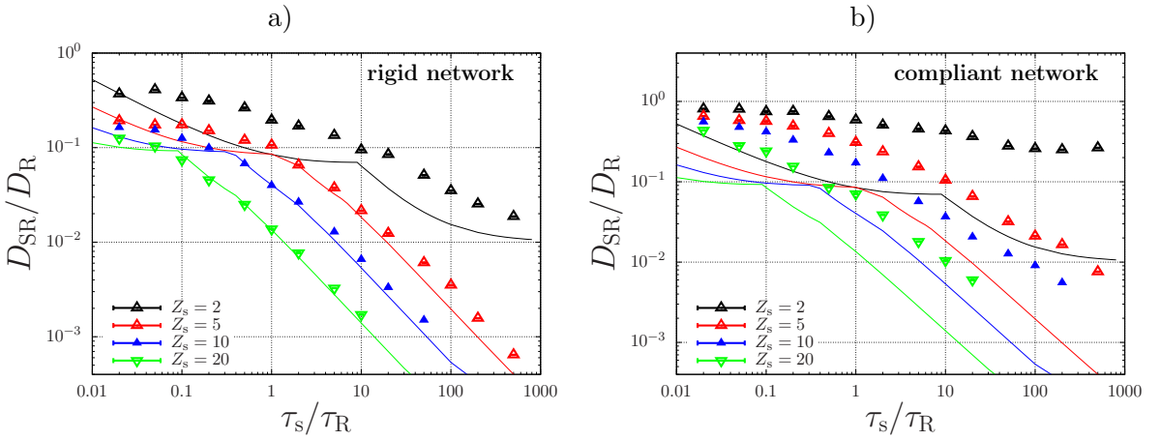

FIG. 6. Sticky Rouse diffusivity, $D_{\rm SR}$, against the sticker lifetime, $\tau_{\rm s}$ for chains with $Z_{\rm s} = 2, 5, 10, 20$ stickers with $p = 0.9$ within a rigid network (a) and a compliant one (b). The symbols are our simulation results, and the curves represents the sticky Rouse model in Ref.[19]. The units are given in terms of the bare Rouse diffusivity $D_{\rm R}$ and the bare Rouse time, $\tau_{\rm R}$.

of various chains within the rigid-network approximation and with a compliant network in Fig. 6. Panel (a) shows that the predictions of Ref.[19] describes our simulations well within the rigid-network approximation for chains with $5, 10, 20$ stickers with various sticker lifetimes, in particular in the regime where the sticky-Rouse diffusivity scales with the sticker lifetime as $D_{\rm SR} = D_{\rm R}\tau_{\rm R}/\tau_{\rm SR} \propto 1/\tau_{\rm s}Z_{\rm s}^2$, see Eq. (32). Panel (b) shows that upon releasing the rigid-network approximation this scaling behaviour persists, but rescaled with a prefactor ≈ 4. While this scaling regime is reached for the chains with more than 5 stickers (i.e., above the percolation threshold for network formation), this is not the case for the chains with 2 stickers. Within the rigid-network approximation, this originates from the fact that at sticker lifetimes a plateau is reached where the chains with all stickers open dominate the dynamics. Without the rigid-network approximation, the chains cluster into linear 'supramolecular' dimers, trimers, etc. through an exponentially decaying cluster-size distribution[69], which implies a distribution of diffusivities that strongly differs from that predicted by the sticky-Rouse model. Hence, while our simulation approach accounts for the elastic compliance of the percolating network, it also captures the contributions of cluster diffusion near and below the percolation threshold for network formation.

B. Non-Linear Dynamics: Steady State

Ordinary Gaussian polymer melts and solutions of narrow molecular-weight distribution exhibit broad conformational distributions in shear flow due to dynamic stretching, tumbling and recoiling of the chains[40–42]. In extensional flow, however, such chains do not tumble and recoil, and their stretch distributions are narrow, see Fig. 7(a). Perhaps surprisingly, by incorporating stickers into the chain these stretch distributions become much wider, see Fig. 7(b). This figure shows that the sticky chains exhibit an enormous dispersity in the chain stretch, as well as occasional hairpin conformations (Fig. 7(b)). These are cause by the stochastic binding and unbinding of stickers, where the network forces may occasionally act in the opposite direction of the drag forces exerted by flow.

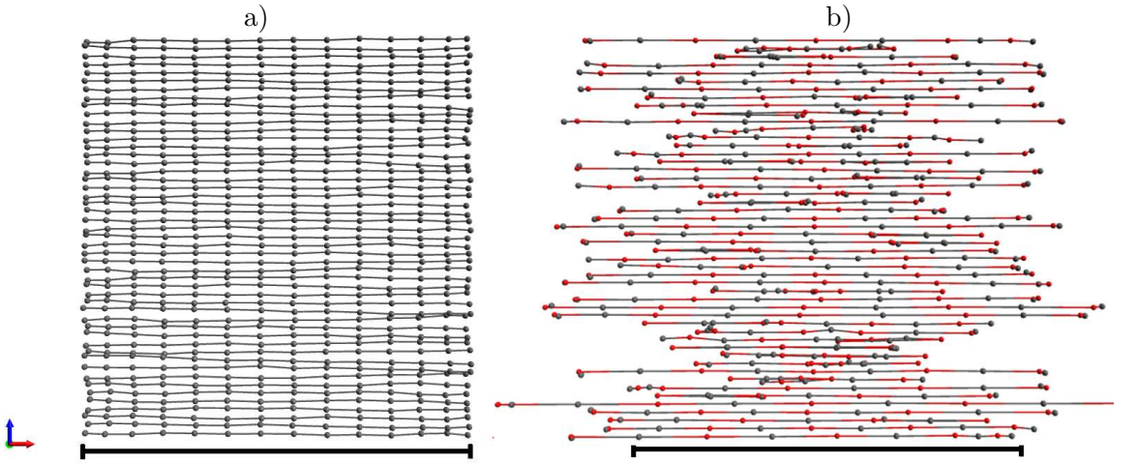

FIG. 7. Representation of simulated chain conformations in extensional flow for $\dot{\varepsilon}\tau_{\mathrm{R}} = 2$ for non-sticky (a) and sticky (b) polymers. While the variations in stretch are narrow for non-sticky polymers, these variations are broad for the sticky polymers: when a sticker in a retracting chain segment binds to a neighbouring chain segment, this may disrupt the neighbouring chain. The scale bar represents approximately a length $50R_{\mathrm{e}}$, which is 65% of the fully extended chain.

To go beyond these qualitative observations, we have quantified this phenomenon using steady-state stretch distributions of polymers at various extension and shear rates in Fig. 8. We have selected non-sticky polymers ($Z_{\mathrm{s}} = 0$), and sticky polymers below ($Z_{\mathrm{s}} = 2$) and above ($Z_{\mathrm{s}} = 5$) the percolation threshold for network formation: The chains with only 2 stickers may only assemble into high-molecular weight chains, while chains with 5 stickers may branch into percolating networks. We have modelled the physics of the stickers using

the same description as in our previous work on chains that are pre-aligned in the flow field[11]. We have summarised the associated parametrisation in the caption of Table I. In extensional flow, above the sticky Weissenberg number, $\mathrm{Wi}^{\mathrm{sticky}} = \dot{\varepsilon}\tau_{\mathrm{SR}}$ with τ_{SR} the sticky Rouse time we expect divergent stretching (albeit that real divergence is obstructed by the maximum chain extensibility $\lambda_{\mathrm{max}} = 75$). We have calculated the sticky Rouse time as $\tau_{\mathrm{SR}} = [D_{\mathrm{R}}/D_{\mathrm{SR}}]\tau_{\mathrm{R}}$, with the ratio between the sticky and the bare diffusivity as presented above in Fig. 6. The relevant results are summarised in Table I.

TABLE I. In our simulations of sticky polymers in non-linear flow conditions we use as parameters $p = 0.9$ as the fraction of closed stickers (in quiescent conditions), a sticker lifetime $\tau_{\mathrm{s}} = 10\tau_{\mathrm{R}}$, an activation energy $E_{\mathrm{act}} = 8k_{\mathrm{B}}T$, and a sticker dissociation length of $\ell = 1$ nm. The maximum extension ratio of the chain is $\lambda_{\mathrm{max}} = 75$. The intramolecular forces in Eq. 5 are calculated by assuming a total number of $N = 5525$ Kuhn segments, and a Kuhn length of $b = 0.4$ nm. As we focus on chains with $Z_{\mathrm{s}} = 2$ and 5 stickers, we here tabulate the ratio between the bare Rouse and sticky Rouse diffusivities, $[D_{\mathrm{R}}/D_{\mathrm{SR}}]$, and relaxation times, $[\tau_{\mathrm{R}}/\tau_{\mathrm{SR}}]$. The diffusivities were determined in Fig. 6, and the sticky Rouse time is calculated as $\tau_{\mathrm{SR}} = [D_{\mathrm{R}}/D_{\mathrm{SR}}]\tau_{\mathrm{R}}$[19].

Polymer model	$D_{\mathrm{SR}}/D_{\mathrm{R}}$	$\tau_{\mathrm{SR}}/\tau_{\mathrm{R}}$
$Z_{\mathrm{s}} = 2$; (rigid)	0.0949 ± 0.0002	10.54 ± 0.02
$Z_{\mathrm{s}} = 5$; (rigid)	0.02156 ± 0.00004	46.38 ± 0.09
$Z_{\mathrm{s}} = 2$; (compliant)	0.4331 ± 0.001	2.309 ± 0.005
$Z_{\mathrm{s}} = 5$; (compliant)	0.1050 ± 0.0002	9.52 ± 0.02

Eq. (4) shows that in all cases the equilibrium stretch distribution for zero-flow conditions (black curve) is approached for small strain rates. For non-sticky chains ($Z_{\mathrm{s}} = 0$), a broad stretch distribution with a cutoff set by λ_{max} emerges in shear due to the dynamic stretching, tumbling and re-collapsing of the chains. In extensional flow, the distribution broadens only within a narrow range of strain rates $0.9 < \dot{\varepsilon}\tau_{\mathrm{R}} < 1.1$ around the bare stretch transition, $\mathrm{Wi} = \dot{\varepsilon}\tau_{\mathrm{R}} = 1$. Beyond the stretch transition, the stretch distribution is narrow and Gaussian and approaches λ_{max} with an increasing strain rate. This behaviour qualitatively changes upon incorporating stickers.

Fig. 8 shows that the steady-state stretch distributions in shear are similar to those of the non-sticky chains, while in extensional flow the distributions of sticky polymers are remark-

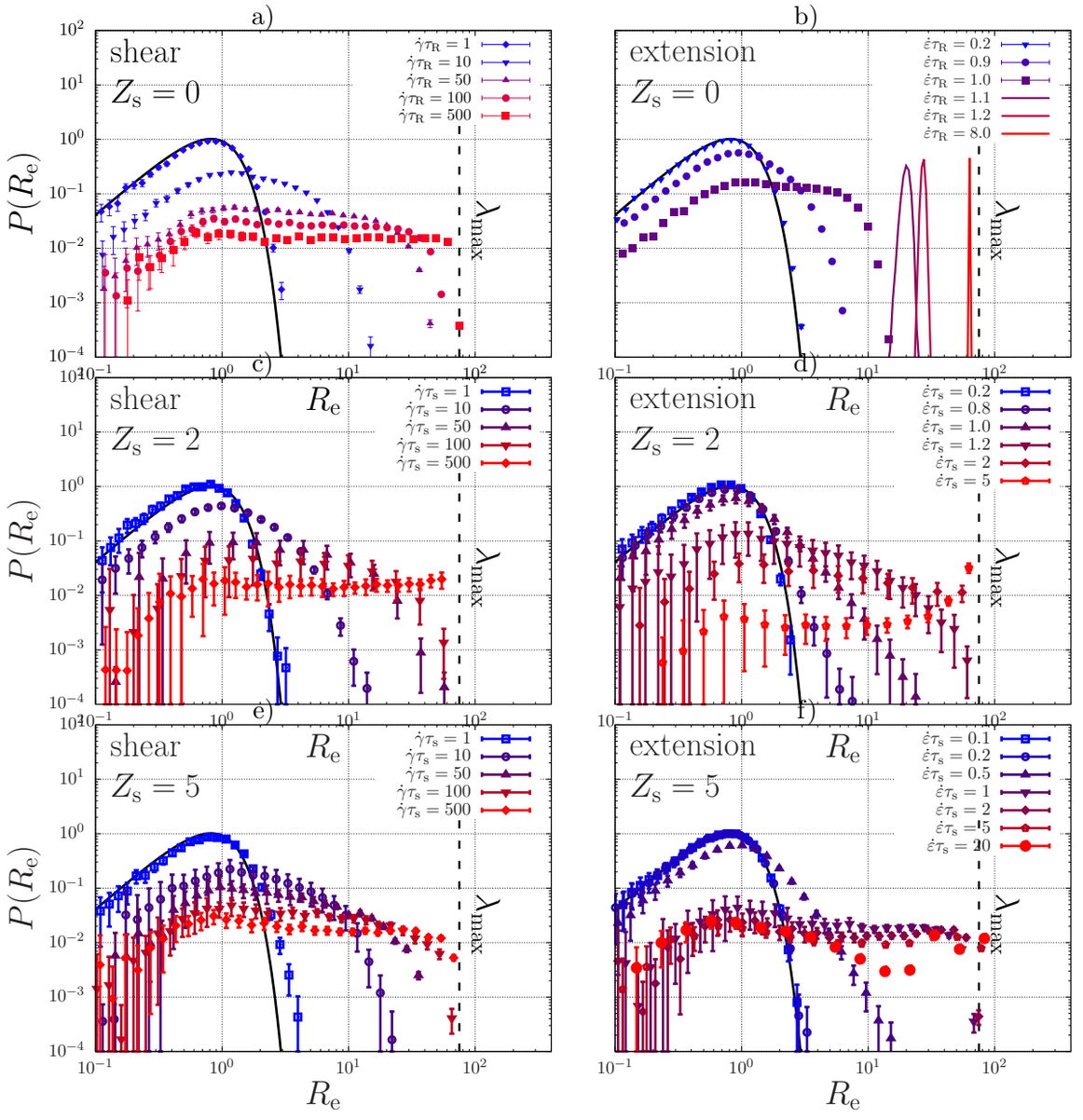

FIG. 8. Simulated steady-state stretch distributions of the end-to-end distance, R_e, for various extension (a,c,e) and shear (b,d,f) rates for a linear unentangled, non-sticky ($Z_s = 0$) and sticky ($Z_s = 2$ and $Z_s = 5$) polymers. For these simulations $\tau_{SR} \approx \tau_s = 10\tau_R$ (see Table I for all parameter values). The black curve represents the contour-length fluctuations in quiescent conditions, given by Eq. (4).

ably distinct from the non-sticky ones: In contrast to the non-sticky polymers, the sticky polymers show broad stretch distributions in steady-state extensional flow over a broad range of flow rates. We have observed this behaviour previously in simulations where the chains

were pre-aligned in the flow-field and where we invoked the rigid-network approximation[11]. Our current simulations show that this phenomenon persists when these approximations are released, but also show a dynamic coexistence of stretched chains, relaxed coils, and hairpins. Interestingly, there is a qualitative similarity between the distributions of the chains with 2 or 5 stickers, despite the fact that these are below and above the percolation threshold for network formation, respectively. This indicates that the enormous reduction of the chain retraction rate due to the stickers does not necessitate network formation: the formation of high-molecular weight assemblies suffices.

We also find that the large fluctuations in stretch below the formal stretch transition carry over from case of 2 stickers per chain to multiple stickers[11]. (The stretch transition is defined at the condition $\dot{\varepsilon}\tau_{\mathrm{SR}} = 1$, with the sticky Rouse time obtained from the sticky-Rouse diffusivity of Fig. 6 as $\tau_{\mathrm{SR}} = \tau_{\mathrm{R}} D_{\mathrm{SR}}/D_{\mathrm{R}}$) In particular, we find that for small strain rates and large stretch ratios λ the stretch distribution has a power-law tail (see Eq. (18)) of which the width is set by a $\dot{\varepsilon}$-dependent stretch exponent ν (see Section II B). We have determined the stretch exponent from the distributions of the chains with 2 and 5 stickers (we discuss the numerical method in Appendix V C) in extensional flow with and without the rigid-network approximation and finite extensibility, and plot these against the strain rate in Fig. 9. As anticipated, we have been able to map the stretch exponent of the chain with two stickers onto the analytical result in Eq. (25). To achieve that, it has to be taken into account that the open state of the chain can be achieved by opening either of the stickers; hence, τ_{s} in Eq. (25), which models the simultaneous opening of all stickers, is replaced by $\tau_{\mathrm{s}}/2$, and results in

$$\nu = -1 - \frac{1}{(1-\dot{\varepsilon}\tau_{\mathrm{R}})}\frac{p}{(1-p)}\frac{2\tau_{\mathrm{R}}}{\tau_{\mathrm{s}}} + \frac{2}{\dot{\varepsilon}\tau_{\mathrm{s}}}. \tag{34}$$

For chains with multiple stickers, no such analytic theory is yet available; however, we do find a qualitative agreement of the increasing power-law exponent with an increasing strain rate.

For the chains with 2 and 5 stickers and with a fraction $p = 0.9$ of closed stickers, we also simulated the stretch distributions while including finite extensibility and an elastically compliant network. Finite extensibility implies that there is a cutoff of the power-law tail, which becomes apparent with increasing (less negative) ν. Since the fluctuations in λ diverge for $\nu \geq -3$, this cutoff has a significant effect on the tail of the stretch distribution upon approaching $\nu = -3$. Fig. 9 does confirm a broadening power-law stretch distribution for

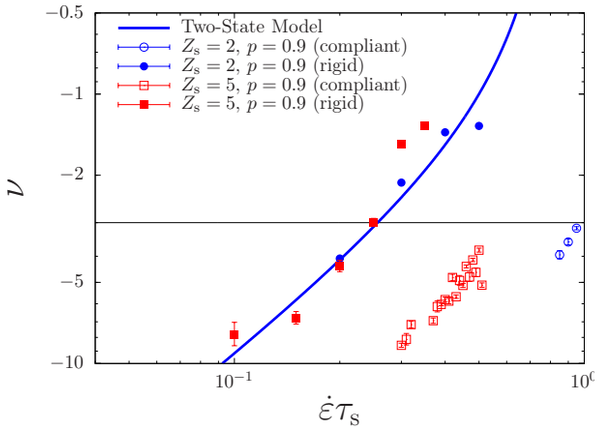

FIG. 9. Stretch exponent ν of the power-law tail of the stretch distribution $P \propto \lambda^{\nu}$ for simulations of polymers with $Z_s = 2$ (blue symbols) and 5 stickers (red symbols), within the rigid-network approximation (closed symbols) and using elastic compliance and finite chain extensibility (open symbols). The solid curve is given by the two-state model in Eq. (34) with $\tau_s = 10\tau_R$ (see Table I for all physical parameter values). For $\nu > -3$ (horizontal line) the fluctuations in stretch diverge; this leads to a cutoff in the stretch distribution for chains with finite extensibility, see Fig. 8.

the chains in a compliant network, but shifted to higher strain rates, as expected from the faster sticky-diffusion rates from Fig. 4.

C. Non-Linear Dynamics: Transients

In our pursuit to understand the flow-induced crystallisation of associating polymers such as the silk protein, we are interested in capturing the macroscopically observable stresses in start-up flow, and to interpret crystallisation rates in terms of the chain conformations that underlie these stresses. To address these challenges, in this section we will present the time-dependent rate-normalised transient shear stress, $\sigma_{xy}/\dot{\gamma}$, and extensional stress $(\sigma_{yy}-\sigma_{rr})/\dot{\varepsilon}$, with the stress tensor (in units of energy per molecule) given by

$$\sigma_{\alpha\beta} = \frac{3k_BT}{b^2N}\sum_{i=1}\Delta s_{i-1}k_{s,i}\frac{Q_{\alpha,i}}{\Delta s_{i-1}}\frac{Q_{\beta,i}}{\Delta s_{i-1}}. \tag{35}$$

Focussing first on the results for non-sticky chains with a finite extensibility $\lambda_{max} = 75$ in Fig. 10(a,b), we reproduce the well-known qualitative features of their stress transient[57]: For small Weissenberg numbers, $\dot{\varepsilon}\tau_R < 1$, $\dot{\gamma}\tau_R < 1$ the polymers are able to relax, while for large

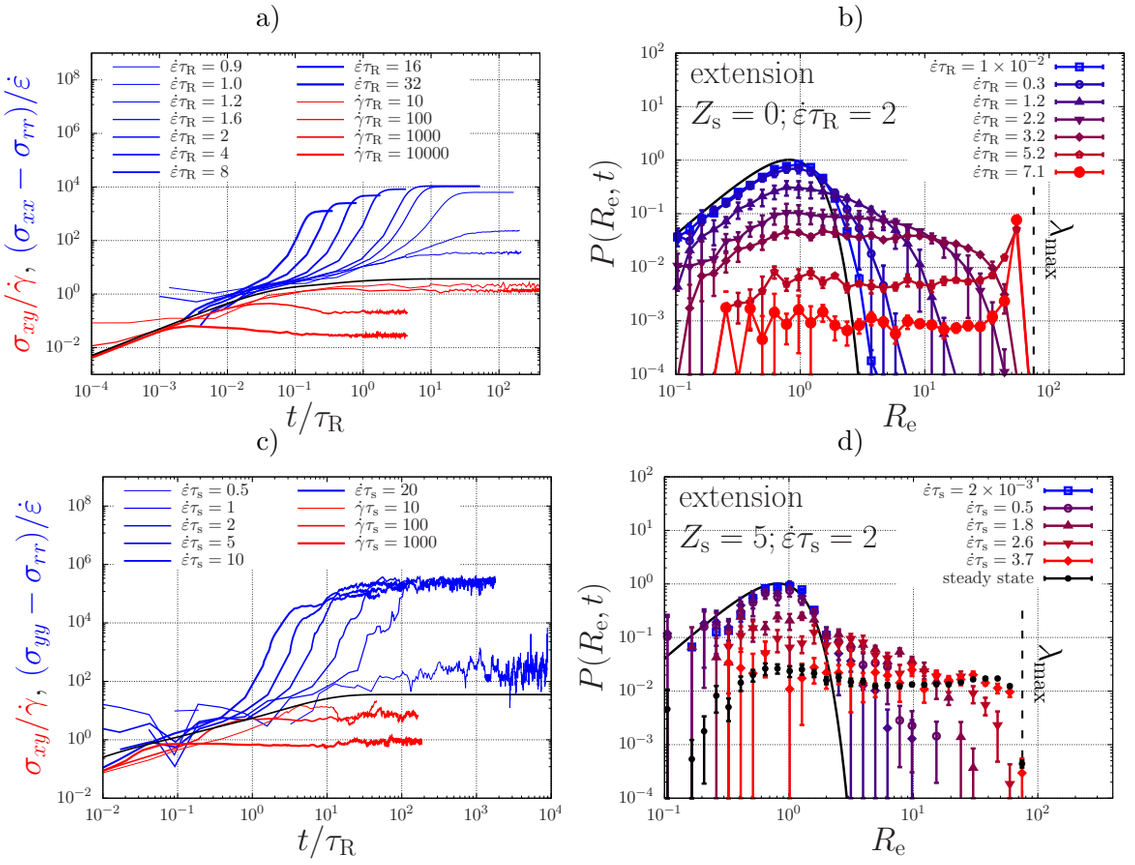

FIG. 10. (a,c) Simulated rate-normalised transient extensional and shear stresses averaged over 50 polymers the non-sticky (a) and the sticky (c) case. The sticky polymer exhibits strong flucuations for $\dot{\varepsilon}\tau_s = 0.5$, which is below the stretch transition (at $\dot{\varepsilon}\tau_s \approx 1$, see Table I). (b,d) Transient stretch distribution of the end-to-end distance, R_e, in extensional flow for the non-sticky (b) and sticky (d) chain at selected strain rates. The error bars in (d) represent half of the standard error of the mean. All physical parameter values are given in Table I.

strain rates there is an overshoot in shear flow, which is related to the onset of tumbling and re-collapsing of stretched chains, and in extensional flow there is a sharp increase in the extensional stress until a plateau due to the finite extensbility of the chains is reached. Because of the thermal fluctuations and dispersity in the initial chain conformations, Fig. 10(b) shows broadening of the stretch distribution at early times. At late times, when all chains are aligned (at the level of the beads), a sharp peak emerges at high stretches near the maximum extensibility λ_{max}.

This sharp peak in the stretch distribution is a fingerprint for non-sticky linear polymers

in extensional flow, and will not be visible for the sticky polymers, as we we will now show for $Z_\mathrm{s} = 5$. We plot the resulting start-up stresses and stretch distributions in Fig. 10(c,d).

Qualitatively, we find similar shear and extensional viscosities as in the non-sticky case, although there is now no distinctive overshoot in shear flow. In extensional flow, the stresses at long time scales have shifted to higher values because of the contribution by the reversible cross-links. Further, while non-sticky polymers show strain hardening only for $\dot{\varepsilon}\tau_\mathrm{R} > 1$, the sticky ones also show strain hardening for smaller strain rates $\dot{\varepsilon}\tau_\mathrm{s} > 1$. For strain rates smaller than that we identify large fluctuations in the transient extensional stress, which are caused by temporary exponential stretching of chain segments between closed stickers that rapidly retract to a near-relaxed state when the stickers open[10]. For strain rates $0.3 < \dot{\varepsilon}\tau_\mathrm{s} < 0.5$ these fluctuations fill up a power-law distribution whose stretch exponent is depicted in Fig. 9. For higher rates, the finite extensibility causes a truncation of this power law tail.

The dynamics by which the stretch distributions evolve in extensional flow above the stretch transition ($\dot{\varepsilon}\tau_\mathrm{s} = 2$) is shown in Fig. 10(d). At early times, the stretch distribution closely resembles the equilibrium distribution of Eq. (4). As time proceeds, a the distribution broadens exponentially with time as $\ln\lambda \propto \dot{\varepsilon}t$ until the steady state is reached after a time $\dot{\varepsilon}\tau \propto \ln\lambda_\mathrm{max}$. This is in qualitative agreement with the predictions of the two-state model that we derived in Eq. (29) of Section II B.

D. Critical specific work

Now that we have captured how stickers lead to broad stretch distributions, we will investigate how these distributions affect the critical work for flow-induced crystallisation (FIC). The usual predictor for FIC is the 'Kuhn segment nematic order parameter', $P_{2,\mathrm{K}} \in [0, 1]$. If $P_{2,\mathrm{K}} \to 1$ (see e.g. Ref. 3), virtually all chains are aligned at the level of the Kuhn segments, i.e., they are completely extended/stretched in the direction of the flow field. However, in this case of high chain-heterogeneity we expect this average measure to be a poor descriptor. We know that the critical nuclei will be dominated by the small fraction of highly-stretched chains, and that it is the oriented segments in these chains only that promote crystallisation. To model this extremum-dominated physics, therefore, we will assume that FIC may commence when a critical fraction, P_s, of chain segments

PLEASE CITE THIS ARTICLE AS DOI: 10.1122/8.0000411

of some length $\Delta s^* \in [0,\, 1]$, have stretched beyond a critical stretch ratio $L_\mathrm{s}\lambda^*_\mathrm{max}$, where $\lambda^*_\mathrm{max} = \lambda_\mathrm{max}\sqrt{\Delta s^*}$ is the maximum stretch of the chain segment and $L^*_\mathrm{s} \in [0,\, 1]$ a parameter that may be viewed as proxy for chain stretch at the Kuhn length of this extremely stretched chain fraction. Hence, the criterion for FIC may within our interpretation be formulated as

$$\int_{L_\mathrm{s}\lambda^*_\mathrm{max}}^{\lambda^*_\mathrm{max}} P(\lambda, t_\mathrm{s})\mathrm{d}\lambda \geq P_\mathrm{s}, \tag{36}$$

where $P(.)$ is the transient stretch distribution function, and t_s is the time into the process of startup flow at which the criterion is satisfied. Essentially, this criterion provides a prediction for the time required to form the first nuclei, and, hence the time t_s should not be confused with the fixed time in FIC experiments[35–37] during which a different number of nuclei may form depending on the strain rate. A comparison to those experiments would require knowledge of the physical relationship between the nucleation rate and the conformational distribution; here, we have proposed a hypothetical condition that is likely to correlate to a fixed nucleation rate. For associating polymers, a natural measure for the length of flow-crystallisable chain segments is $\Delta s^* = 1/(Z_\mathrm{s} + 1)$; in general, however, measures for P_s, L_s, and Δs^* will have to be determined through experimentation and (atomistic) MD simulations[15–18].

In this section, we will employ simulations with 50 chains of a fixed number of 11 beads (i.e., with 10 chain segments, giving $\Delta s^* = 1/10$), and we will monitor the maximum stretch among the total of 500 chain segments (i.e., $P_\mathrm{s} = 1/500$). The time-evolution of the maximum stretch will enable us to screen how various values of L_s require a different processing time t_s and a different input of specific energy. We obtain statistics on this relationship by averaging our results over 5 simulations with different initialisation 'seeds' of the random-number generator. We will discuss the implications of the criterion in Eq. (36) by comparing it to a measure of the (mean-field-type) nematic order parameter. At our level of coarse graining, the highest resolution of nematic chain alignment is captured using the nematic order parameter $P_{2,\mathrm{s}} \in [0, 1]$, which is the largest eigenvalue of the nematic order tensor $\mathbf{P}_{2,\boldsymbol{s}} = (3\langle\mathbf{uu}\rangle - 1)/2$, where $\mathbf{u}$ is the unit vector tangential to the backbone of the chain. (we remark that this nematic order parameter is an overestimate of the Kuhn segment nematic order, i.e., $P_{2,\mathrm{s}} > P_{2,\mathrm{K}}$) In Fig. 11, we have calculated the critical specific work, W, as given in Eq. (1), needed to achieve values of $P_{2,\mathrm{s}}$ and L_s in the range from 0 to

1 for non-sticky ($Z_s = 0$) and sticky ($Z_s = 5$) chains for various shear and extensional rates.

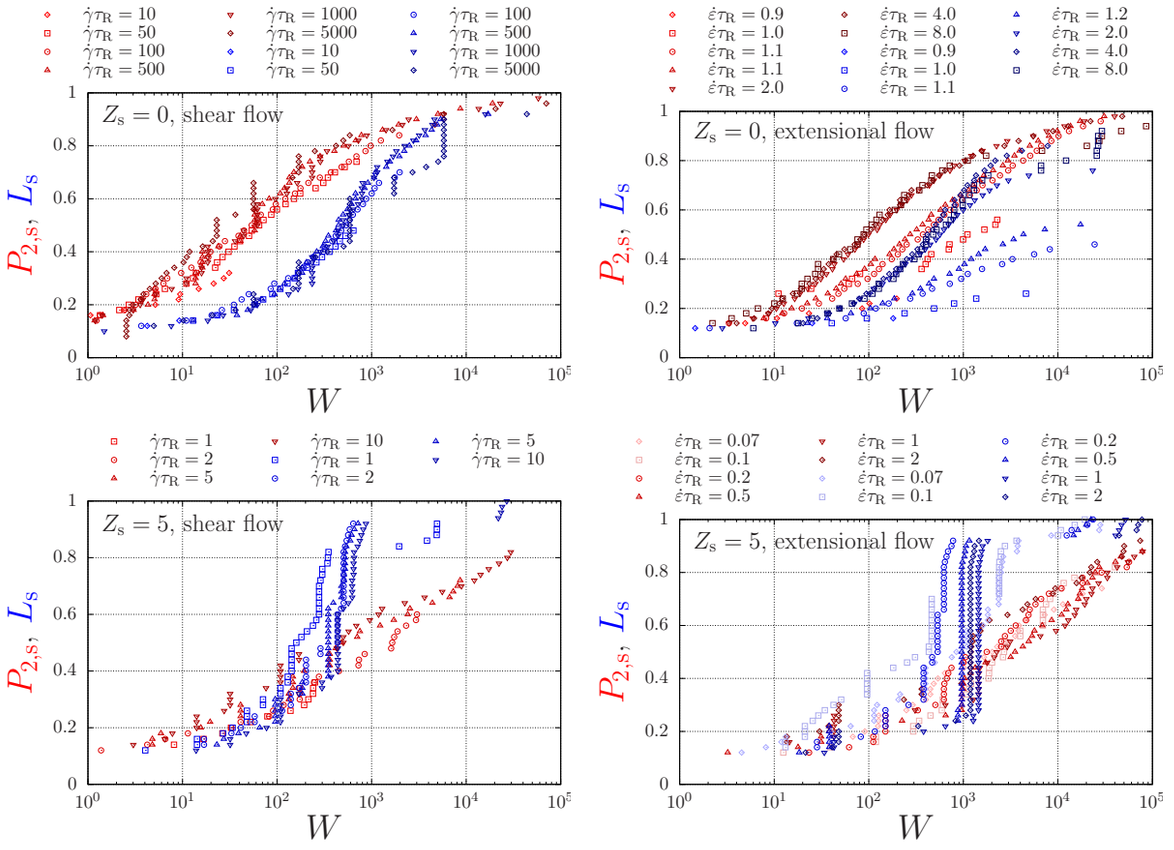

FIG. 11. Nematic order parameter, $P_{2,s}$ and characteristic stretch ratio, L_s, against the specific work (see main text) for sticky (red) and non-sticky (blue) polymers in shear (left) and extensional (right) flow. The symbols are obtained from simulations with various strain rates for a chain with $Z_s = 5$ with an elastically compliant network. All physical parameter values are given in Table I.

The top panels of this Figure give the nematic order parameter, $P_{2,s}$, and the measure for stretch fluctuations, L_s against the critical specific work. For large values of the critical work, both measures converge, which suggests that both measures can interchangeably used as predictors for flow-induced crystallisation for non-sticky chains. We notice that the critical work in shear (left) and extensional flow (right) show similar trends well above the stretch transition (the stretch transition of the bare chain is $\dot{\varepsilon}\tau_R = 1$). Just above this transition the critical work required is relatively large. This implies a monotonically decreasing critical work with an increasing strain rate, which is due to the suppression of energy dissipation by recoiling of the chains (we discuss this in more detail in Fig. 12). This

PLEASE CITE THIS ARTICLE AS DOI: 10.1122/8.0000411

is in contrast to the typical behaviour in experiments on non-associating polymers (e.g., the flow-induced crystallisation of HDPE[7]), where the critical work *increases* with an increasing strain rate. We argue this discrepancy occurs because we here consider unentangled rather than entangled chains. Finally, the top panels of Fig. 11 confirm the expected behaviour where the nematic order parameter (red) is typically larger than the stretching parameter (blue): with an increasing specific work the chains first align and then stretch.

This behaviour is crucially altered for the sticky polymers, as shown in the bottom panels of Fig. 11. We find that the alignment of the chains requires more critical work both in shear (left) and extensional flow (right), which is due to the fact that the full alignment of the chains requires the opening of intermolecular associations. On the other hand, the stretching of chain segments can take place before global chain alignment. (Note that the stretch transition is $\dot{\varepsilon}\tau_{\mathrm{R}} \approx 0.1$ for this system, see Table I) The stretching parameter (blue) follows a sharp sigmoidal dependence against the critical work, and rapidly outgrows the alignment parameter (red) This is possible because the stretching parameter provides information about a fraction $P_{\mathrm{s}} = 1/500$ of chains in the tail of the distribution, while the alignment parameter provides information about the mean properties. This supports out hypothesis that flow-induced crystallisation may be achieved at a small critical specific work by exploiting the stochastic nature of associating polymers.

Given either a L_{s} or $P_{2,\mathrm{s}}$ criterion for critical nucleation, we are interested how the strain rate affects how much critical specific work, W, is needed, and at what timescale, t_{s} this criterion is achieved. To investigate this, we focus on horizontal lines / cross sections of Fig. 12 (i.e., at fixed values 0.6 and 0.8 of both L_{s} and $P_{2,\mathrm{s}}$). For the data points along these lines we plot the critical workk, W, and the timescale, t_{s}, in Fig. 12. The left panel shows that the timescale scales as $t_{\mathrm{s}} \propto \mathrm{Wi}^{-1}$, as one may expect and discuss in more detail below. Below the stretch transition this dependence becomes stronger: under these conditions many chain stretches are attempted, but fail due to sticker opening and lead to energy dissipation through chain retraction. This crossover between two regimes qualitatively agrees with that found in Figure 2 of the work by Holland et al. on silk[7]; more dedicated research is needed to investigate this observation.

The right panel of Fig. 12 shows the critical specific work needed to achieve a certain degree of alignment, $P_{2,\mathrm{s}}$ (red), or of stretch fluctuations, L_{s} (blue), in shear (open symbols) and extensional flow (closed symbols), against the sticky Weissenberg number. Evidently, a

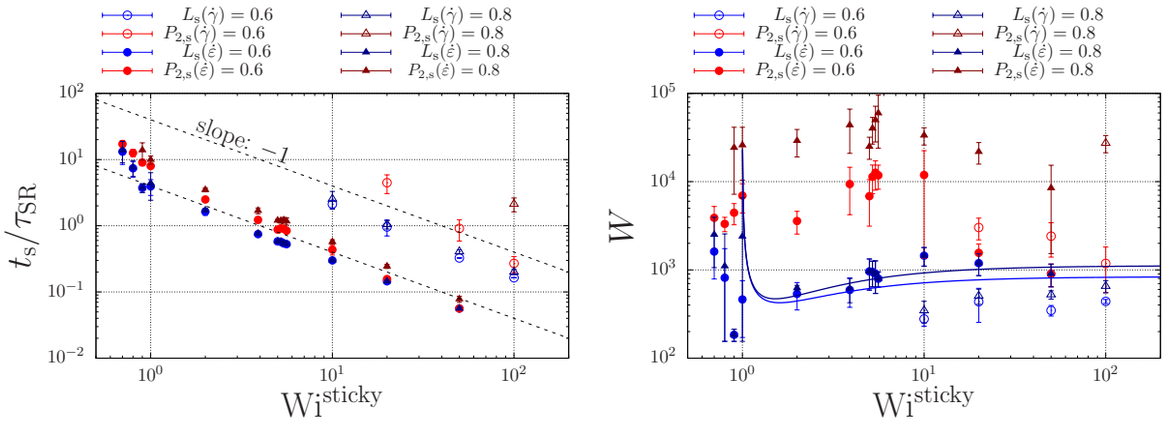

FIG. 12. The critical time (left) and the specific critical work (right) against the sticky Weissenberg number, $\mathrm{Wi}^{\mathrm{sticky}} = \dot\varepsilon\tau_{\mathrm{SR}}, \dot\gamma\tau_{\mathrm{SR}}$, for various L_s and $P_{2,s}$ criteria for the critical condition. The open symbols were calculated in shear and the closed ones in extensional flow. The values are obtained for a chain with $Z_s = 5$ with an elastically compliant network. It is useful to interpret the strain rates in relation to the stretch transition for the sticky chains in extension at $\mathrm{Wi}^{\mathrm{sticky}} = 1$, where the 'sticky' Weissenberg number is $\mathrm{Wi}^{\mathrm{sticky}} \approx 10\mathrm{Wi} = 10\dot\varepsilon\tau_{\mathrm{R}}$, with Wi the Weissenberg number of the non-sticky chain. This factor 10 is non-universal and depends on the number and lifetime of stickers, see Table I for all physical parameter values. The solid curves are given by Eq. (40) for $L_s = 0.6$ and for $L_s = 0.8$.

high degree of overall alignment / nematic order requires much larger specific work than a small fraction of large stretch fluctuations does, as discussed in Fig. 11. Having in mind our overarching proposition that crystallisation may occur in response to stretch fluctuations, we now focus on the measure for L_s. We remark that for the system we studied, the stretch transition in the absence of stickers takes is located at $\mathrm{Wi}^{\mathrm{sticky}} = \dot\varepsilon\tau_{\mathrm{SR}} \approx 10$ (because $\tau_{\mathrm{SR}} \approx 10\tau_{\mathrm{R}}$, see Table I). For smaller strain rates, $\mathrm{Wi}^{\mathrm{sticky}} < 10$, we find there is a minimum in the specific critical work near the stretch transition $\mathrm{Wi}^{\mathrm{sticky}} \approx 1$. Indeed, while large stretches are achieved just below the stretch transition $\mathrm{Wi}^{\mathrm{sticky}} < 1$ due to long power-law tails in the stretch distribution[10], many of attempt fluctuations are needed before the required stretch value is achieved. Due to the energy dissipation of such unsuccesful attempts, the specific critical work increases for decreasing strain rates. Above the minimum, the specific work increases and eventually reaches a plateau.

We explain the increase of the critical specific work with an increasing strain rate in terms

of the two-state model that we introduced in the Theory section. We argue that the stress is dominated by the contributions of stretched chains in the closed state,

$$\sigma_{xx}(t) = c \int P_0(\lambda, t)\lambda(t)^2 \mathrm{d}\lambda, \tag{37}$$

with c a constant, assuming that the open chains are in a relaxed state. Here, $P_0(\lambda, t)$ is the stretch distribution of the closed chains, of which we will discuss the dynamics below. We will then calculate the critical specific work as $W = \int_0^{t_\mathrm{s}} \sigma_{xx}\dot{\varepsilon}\mathrm{d}t$. To calculate W, we first will determine t_s using the criterion

$$\int_{L_\mathrm{s}\lambda_{\mathrm{max},i}}^{\lambda_{\mathrm{max},i}} P_0(\lambda, t_\mathrm{s})\mathrm{d}\lambda \geq P_\mathrm{s}, \tag{38}$$

which, as before, implies a minimum concentration of chains with a stretch ratio of at least $\lambda_\mathrm{s} = L_\mathrm{s}\lambda_{\mathrm{max},i}$. Secondly, we will need an expression for the time evolution of the probability density P_0.

To obtain P_0, we will assume that all chains that have (temporarily) opened are sufficiently relaxed compared to the most stretched chains to have a negligible contribution to the overall stress σ_{xx}. Therefore, we will only take into account the loss of strongly stretched chains by opening rate k_open, and ignore the contribution of closing events by rate k_close. We will further use the initial condition $P(\lambda, 0) = \delta(1-\lambda)$, with $\delta(.)$ the Dirac delta distribution to represent a narrow stretch distribution at time $t = 0$. The dynamical equation in Eq. (21) then predicts that the Dirac delta distribution in time shifts to high stretch values along the λ axis, as

$$P_0(\lambda, t) = \delta(\ln\lambda - \dot{\varepsilon}t)\lambda^{-(1+1/(\dot{\varepsilon}\tau_\mathrm{s}))}, \tag{39}$$

with an amplitude that decreases in time due to sticker opening (we present the derivation in the first two paragraphs of Appendix V B).

Eq. (39) shows that the critical stretch and the critical time are related by $t_\mathrm{s} = \ln\lambda_\mathrm{s}/\dot{\varepsilon}$, which is in agreement with our simulated results displayed in Fig. 11. We insert this equation into the expression for the critical specific work, $W = \int_0^{t_\mathrm{s}} \sigma_{xx}\dot{\varepsilon}\mathrm{d}t$, and find

$$W(\dot{\varepsilon}) = c\left(1 - \frac{1}{\dot{\varepsilon}\tau_\mathrm{s}}\right)^{-1} \exp\left[\left(1 - \frac{1}{\dot{\varepsilon}\tau_\mathrm{s}}\right)\ln\lambda_\mathrm{s} - 1\right], \quad \text{for} \quad \dot{\varepsilon} > \dot{\varepsilon}_\mathrm{min}, \tag{40}$$

where $\dot{\varepsilon}_\mathrm{min}$ is the minimum strain rate for which the criterion in Eq. (38) is obeyed. This function is plotted in Fig. 12(b). It diverges at $\dot{\varepsilon}\tau_\mathrm{s} = 1$ (this divergence is not followed

by the simulation data, because stochastic closing events that generate new bound chain segments), reaches a minimum, and then monotonically increases towards a plateau value. Physically, this plateau value represents the case where the entire distribution of chains is stretched to reach the critical stretch value λ_s. In this case, the concentration of stretched segments far exceeds the critical concentration, and more energy has been put into the system then needed. By decreasing the strain rate, an increasing number of stickers are able to open and the stress is relaxed, in turn decreasing the critical specific work to achieve the critical condition in Eq. (38). This supports our proposition that the stochastic nature of the binding and unbinding of associations enables to molecularly engineer associating polymers to undergo flow-induced crystallisation at low energetic costs. In particular, we have shown, using simulations and an approximate theory in Eq. (40) that there is an *optimum* strain rate at which the critical work for critical stretch is minimised

IV. DISCUSSION AND CONCLUSIONS

This work has shown that the transient evolution of the chain-stretch distribution of associating 'sticky' polymers in shear, and especially extensional, flow possesses an extremely rich structure. The theoretical and numerical investigations reported here were driven by the observation that the silk protein (i) undergoes efficient, chemically tunable, flow-induced crystallisation and (ii) can be modelled as an associating/sticky polymer. Our findings have implications for the interpretation of silk-spinning data, as well as to the development of novel associating polymers and the computational modelling tools (we introduced a 'sticky' sliplink model, and an analytical two-state master equation which may be transferable to also address the peculiar dynamics of ring polymer in flow[43–45]).

Regarding silk rheology, we have theoretically confirmed our hypothesis that the stickers between chains may reduce the critical specific work to induce flow-induced crystallisation (FIC) under reasonable assumptions for critical crystallisation criteria. In our approach, we have adopted the view that FIC may commence when a sufficient concentration of chains is aligned at the level of the Kuhn segments. However, in contrast to the ensemble-averaged approach where the Kuhn segmental nematic order parameter is measured as a predictor for FIC, we have assumed that a critical concentration of strongly stretched chain segments *in the tail of the distribution* is a sufficient condition for crystallisation. Indeed, by comparing a

measure for the stretch fluctuations to the (ensemble-average) nematic order parameter, we have found that the stickers hamper initial chain alignment (chain alignment is slowed down by the need for stickers to dissociate), while segmental stretch is facilated by the closed stickers. Importantly, our analysis revealed that the incorporation of stickers enables a significant reduction in the input of specific work needed to achieve large stretch fluctuations, and consequently, may reduce the energy requirements for FIC.

Focussing on our finding that chain alignment at low, non-stretching, flow rates requires less specific work in the absence of stickers (and presumably for low sticker lifetimes) than with stickers, while the stretching of the chains at high rates is helped by long sticker lifetimes, we speculate that control over both the structural aspects of the final material and over the specific work needed is possible through time- or position-dependent sticker lifetimes. We argue this can be achieved through external chemical control. Indeed, during its larval life cycle, the silkworm stably stores its silk solution at a high viscosity, but just prior to silk spinning it lowers the viscosity through an increase of the potassium concentration through a decreasing lifetime of calcium bridges (stickers)[8,9]. This, as we can now interpret as a mechanism to ease chain alignment in flow. Intriguingly, downstream the spinning duct the acidity increases[34], which we expect to increase the stability and hence the lifetime of the calcium bridges, and hence enhance local chain stretching, see Fig. 1, which may in turn disrupts the solvation layer of the protein and induce efficient crystallisation[7,13,15–18].

While this seems a compelling mechanism for efficient flow-induced crystallisation, it is not yet clear how this process may be optimised. The experimental accessibility of these and other questions has come in reach owing to recent advances in controlling the content of metal cations in silk feedstock[70]. In the case of *Bombyx mori* silk, we identified a regular spacing of the negative charges along the backbone of the chain, with strands of approximately 500 uncharged amino acids between; the length of these sticker strands is of the order of the entanglement molecular weight[9]. The regularity of the spacing and the coincidental similarity between the number of stickers and entanglements suggests some degree of evolutionary optimisation. The functionality of ordered- versus random co-polymers is of high importance from a synthetic polymer chemistry point of view, and needs to be addressed using simulations that include both associations and entanglements.

We conclude that our modelling approach leaves us well prepared to investigate the ways in which the evolution of silk-producing organisms may have exploited the potential optimal

strategies for efficient fibre processing. The next piece of physics to add to this account of the rheology of polymers with temporary assocations, not only for modelling silk proteins but also general associating polymers, concerns the interaction between entanglements and associations in strong flow. We anticipate that this will further enrich the ongoing debate in polymer physics on the physics of entanglement generation and destruction (i.e., 'entanglement stripping') in non-linear rheo-physics, as well as continue the account of how silk-forming organisms point to novel rheo-physics of flow-induced phase-transformations.

V. APPENDIX

A. Algorithm

Because of the large distribution of chain stretch in the conditions we are interested in, there is also a large distribution of opening rates; in our previous work we used small time steps in which the chain conformation was updated, and each closed pair had a sufficiently small opening probability. Here, we significantly improve this algorithm by enabling much larger time steps between conformational updates, and during which the stickers may open and close many times, see Fig. 3.

In our algorithm, we update the *chain conformation* using the Brownian dynamics equation from the previous section using a time span Δt. Depending on the opening and closing rates, during this time span, $\Delta t_1 \equiv \Delta t$, the *sticker configuration* may be updated many times or not at all according to a kinetic Monte Carlo (kMC) scheme[64–66]. In every kMC step, the rate at which any opening or closing event may occur is calculated as $W_\mathrm{T} = W_\mathrm{a} + W_\mathrm{d}$, with

$$W_\mathrm{a} = k_\mathrm{a} N_\mathrm{open}(N_\mathrm{open} - 1)/2, \tag{41}$$

the sum of closing rates and

$$W_\mathrm{d} = \sum_{q=1}^{N_\mathrm{closed}/2} k_{\mathrm{d,q}}, \tag{42}$$

the sum of dissociation rates, where $k_{\mathrm{d,q}}$ differs for the different sticker pairs due to dispersity in chain tension. In these expressions, N_open and N_closed are the number of open and closed stickers, respectively; $N_\mathrm{open}(N_\mathrm{open} - 1)/2$ is the total number of possible associations, and the index q sums over all $N_\mathrm{closed}/2$ *pairs* of closed stickers. Using this sum of rates, the time

Δt_2 at which the first opening or closing event occurs is

$$\Delta t_2 = -\frac{1}{W_\mathrm{T}} \ln(u), \tag{43}$$

with $u \in (0, 1]$ a uniform random number (our code uses random numbers using the open-source SFMT library[71]). If Δt_2 exceeds the time span Δt_1, no opening or closing events occurs. However, if $\Delta t_2 < \Delta t_1$ then a second random number $\in [0, 1]$ is drawn, and a closing event is selected with probability $k_\mathrm{a}/W_\mathrm{T}$, and a dissociation event q is selected with probability $k_\mathrm{d,q}/W_\mathrm{T}$. After updating the configurations of the stickers, the time span is updated to $\Delta t_1 = \Delta t_1 + \Delta t_2$. The kMC scheme is terminated when $\Delta t_2 > \Delta t_1$, following which the chain conformation is updated.

While in the linear rheological conditions we solve the dynamics using a fixed time step, in strong flow we implemented an adaptive time step to handle the large and fast fluctuations in stretch that emerge in some parameter regimes of the system. In every iteration n, the time step for the next iteration is updated as

$$\Delta t^{n+1} = \Delta t^n \left(\min_{Q_i} \frac{\text{tolerance}}{\text{error}} \right)^{0.25}, \tag{44}$$

where an error and tolerance are calculated for the change of each end-to-end vector $\mathbf{Q}_i$. We defined the error value for each change in Q_i as error $= |\Delta Q_i^n|/Q_\mathrm{max}$, with Q_max set by λ_max. For the tolerance value we use scalar values tol_- and tol_+ depending on whether $|Q_i^n|$ is smaller or larger than a certain cutoff set by $\lambda_\mathrm{cutoff} < \lambda_\mathrm{max}$. Above the cutoff, we avoid numerical instabilities due to the singularity at λ_max by using

$$k_\mathrm{s}(\lambda > \lambda_\mathrm{cutoff}) = k_\mathrm{s}(\lambda_\mathrm{cutoff}) \times \left(\frac{\lambda}{\lambda_\mathrm{cutoff}} \right)^\alpha. \tag{45}$$

For continuity of the derivative, $\alpha = 4c^2/(3 - 4c^2 + c^4)$, with $c = \lambda_\mathrm{cutoff}/\lambda_\mathrm{max}$; for a cutoff $\lambda_\mathrm{cutoff} = 0.9\lambda_\mathrm{max}$ even this smooth potential is steep ($\alpha \approx 8$), and in practice we use a softer potential ($\alpha = 4$).

B. Asymptotic limits of the two-state model

The two-state master equation in Eqs. (21-22) has analytical solutions for early times where advection dominates over the sticker dynamics, and for late times where the sticker dynamics is fast compared to the rate by which the deep tail of the stretch distribution

fills up. We obtain these analytical solutions in both cases using the Laplace transform of Eqs. (21-22) in the limit of large stretches $\lambda > \lambda_* \gg 1$, which is

$$\frac{\partial \tilde{P}_0}{\partial y} = -(k_{\rm open} + \dot{\varepsilon} + s)\tilde{P}_0 \qquad +k_{\rm close}\tilde{P}_1 + P_0(0,y)/s, \tag{46}$$

$$\frac{\partial \tilde{P}_1}{\partial y} = +k_{\rm open}\tilde{P}_0 \qquad -(k_{\rm close} + \dot{\varepsilon} + s - \tau_{\rm R}^{-1})\tilde{P}_1 + P_1(0,y)/s, \tag{47}$$

where $\tilde{P}_i(s,y) \equiv \mathcal{L}\{P_i(t,y)\}$ is the Laplace transform of P_i for $i = 0, 1$ (hence, we have used the standard Laplace transform of the time derivative $\mathcal{L}\{\partial P_i/\partial t\} = s\tilde{P}_i(s,y) - P_i(0,y)$). We will obtain the early- and late-stage solutions by using different initial conditions $P_i(0,y)$ at $t = 0$ and boundary conditions that we will discuss below.

Focussing first on the early-stage limit, we consider a narrow distribution $P(\lambda, 0) = \delta(1 - \lambda_*)$ of chain segments between closed stickers at time $t = 0$, with $\delta(.)$ the Dirac delta distribution. For early times, these segments stretch exponentially with time until the stickers open. To inspect how these segments evolve, we insert the initial conditions into Eq. (46), which gives

$$\frac{\partial \tilde{P}_0}{\partial y}(\lambda, s) = -(k_{\rm open} + \dot{\varepsilon} + s)\tilde{P}_0(\lambda, s) + c\delta(1 - \lambda), \tag{48}$$

with $\tilde{P}_0(\lambda, s)$ the Laplace transform of $P_0(\lambda, s)$. The solution is of the standard form $\tilde{P}_0 \propto \exp(-s\tau)$, which after inverse Laplace transform gives Eq. (39) in the main text.

To solve Eqs. (21-22) in the long-time limit, we make the useful approximation that at an intermediate time $t = t_*$ the distribution is at steady state for small stretches $\lambda \leq \lambda_*$, while the large-stretch tail of the distribution is unoccupied. Hence, at $t = t_*$ the distribution is given by

$$P_0(0,y) = \frac{c'}{c} P_0^{\rm eq}\Theta(-y + y_*) \tag{49}$$

$$P_1(0,y) = \frac{c'}{c} P_1^{\rm eq}\Theta(-y + y_*), \tag{50}$$

where $y_* \equiv \ln \lambda_*$ and where Θ is the Heaviside step function. The prefactor

$$c' = \left(1 + c\frac{1}{1+\nu}\mathrm{e}^{(1+\nu)y_*}\right)^{-1} > 1, \tag{51}$$

normalises the distribution. We now set λ_* to a large value, so $c' \approx c$, and at late times $t > t*$ the filling of the tail of the distribution (for $\lambda > \lambda_*$) occurs with a negligible effect on the distribution at small stretches.

of which the solution is of the form

$$\tilde{P}_0(s,\lambda) = c_0^+(s)\lambda^{\nu_+(s)} + c_0^-(s)\lambda^{\nu_-(s)} \tag{52}$$

$$\tilde{P}_1(s,\lambda) = c_1^+(s)\lambda^{\nu_+(s)} + c_1^-(s)\lambda^{\nu_-(s)}, \tag{53}$$

with $\nu_-(s)$ and $\nu_+(s)$ the eigenvalues given by

$$\nu_\pm = \frac{1}{2\dot{\varepsilon}(1-\dot{\varepsilon}\tau_\mathrm{R})}\Big((2\dot{\varepsilon}+k_\mathrm{open})(1-\dot{\varepsilon}\tau_\mathrm{R}) - \dot{\varepsilon}\tau_\mathrm{R}k_\mathrm{close} + s(1-2\dot{\varepsilon}\tau_\mathrm{R}) \pm\sqrt{(s+k_\mathrm{open}(1-\dot{\varepsilon}\tau_\mathrm{R}))^2 + 2\dot{\varepsilon}\tau_\mathrm{R}(s-(1-\dot{\varepsilon}\tau_\mathrm{R})k_\mathrm{open})k_\mathrm{close} + (\dot{\varepsilon}\tau_\mathrm{R}k_\mathrm{close})^2}\Big), \tag{54}$$

and where the coefficients, $c_i^\pm$, follow from the boundary condition at $y = y_*$.

At late times, i.e., for small s, we have $\nu_-(s) \approx \nu_\mathrm{eq} - (s/\dot{\varepsilon})\nu' + (1/2)(s/\dot{\varepsilon})^2\nu''$, where ν_eq is given by Eq. (25), and where

$$\nu' \equiv \left.\frac{\mathrm{d}\nu}{\mathrm{d}(s/\dot{\varepsilon})}\right|_{s=0} = \left(1 - \frac{1}{1-\mathrm{Wi}} + \frac{1}{1-\mathrm{Wi}^\mathrm{sticky}}\right), \tag{55}$$

and

$$\nu'' \equiv 2p\mathrm{Wi}\frac{\mathrm{Wi}^\mathrm{sticky}}{(1-\mathrm{Wi}^\mathrm{sticky})^3}, \tag{56}$$

are both positive, provided that the sticky Weissenberg number is sufficiently small, $\mathrm{Wi}^\mathrm{sticky} \equiv \mathrm{Wi}/(1-p) < 1$[10], where $\mathrm{Wi} = \dot{\varepsilon}\tau_\mathrm{R}$ is the Weissenberg number of the chain without stickers.

From the boundary condition, we find that the coefficients must be of the form $c_i^\pm \propto 1/s$. As the '+' solution leads to a non-normalisable solution, however, $c_i^+ = 0$, and the solution is

$$\tilde{P}_0(s,\lambda) = \frac{c}{s}(\lambda/\lambda_*)^{\nu_- - (s/\dot{\varepsilon})\nu' - \frac{1}{2}(s/\dot{\varepsilon})^2\nu'' + \mathcal{O}(s^3)}, \tag{57}$$

$$\tilde{P}_1(s,\lambda) = \frac{k_\mathrm{close}}{k_\mathrm{open}}\frac{\dot{\varepsilon}}{(\dot{\varepsilon}-\tau_\mathrm{R}^{-1})}\tilde{P}_0(s,\lambda). \tag{58}$$

Finally, after taking the inverse Laplace transform, we have

$$P_0(t,\lambda) = c\left(\frac{\lambda}{\lambda_*(0)}\right)^{\nu_\mathrm{eq}}\Theta(\nu'\ln\lambda/\lambda_* - \dot{\varepsilon}t) \tag{59}$$

$$P_1(t,\lambda) = \frac{k_\mathrm{close}}{k_\mathrm{open}}\frac{\dot{\varepsilon}}{(\dot{\varepsilon}-\tau_\mathrm{R}^{-1})}P_0(t,\lambda). \tag{60}$$

Hence, the exponentially extending front of the distribution is located at the stretch ratio

$$\lambda_*(t) = \lambda_*(0) \exp\left[\left(1 - \frac{1}{1-\mathrm{Wi}} + \frac{1}{1-\mathrm{Wi}^{\mathrm{sticky}}}\right)^{-1} \dot{\varepsilon}(t - t_*)\right]. \tag{61}$$

We have checked the validity of our interpretation of a narrow moving-front by also calculating the width of this front. To do this, we consider the relaxation function $f(t) = P(y,t)/P_{\mathrm{eq}}(y)$ with again $y = \ln\lambda$, and P and P_{eq} the transient and steady-state stretch distributions, respectively. A narrow front that reaches y at time τ and reaches a steady state at time $\tau + \Delta$ may be approximated by

$$f(t) = \begin{cases} 0, & \text{for} \quad t < \tau \\ (t-\tau)/\Delta, & \text{for} \quad \tau \le t < \tau + \Delta \\ 1, & \text{for}, \quad t \ge \tau + \Delta. \end{cases} \tag{62}$$

The Laplace transform of this function is

$$\mathcal{L}\{f\} = \frac{1}{s^2\Delta} \mathrm{e}^{-s\tau}\left(1 - \mathrm{e}^{-s\Delta}\right). \tag{63}$$

We compare this result to the solution of the two-state model in Eq. (54) through a second-order Taylor expansion of the exponential terms

$$\mathcal{L}\{f\} = \frac{1}{s}\Big(1 - \underbrace{(\tau + \frac{1}{2}\Delta)}_{(\nu'/\dot{\varepsilon})\ln y} s + \frac{1}{2}\underbrace{(\tau^2 + \frac{1}{3}\Delta^2 + \Delta\tau)}_{(\nu''/\dot{\varepsilon}^2)\ln y} s^2\Big). \tag{64}$$

From the linear term, we find $\tau + \Delta/2 = (\nu'/\dot{\varepsilon})\ln y$ (as expected from Eq. (29)). After substitution into the second term and elimination of this variable, we find the width of the front to be

$$\Delta = \sqrt{12}\sqrt{(\nu''/\dot{\varepsilon})\ln y - (\nu'/\dot{\varepsilon})^2 \ln y}. \tag{65}$$

The relative width, compared to the location of the front $(\tau + \Delta/2)$, is

$$\Delta_{\mathrm{rel}} \equiv \frac{\Delta}{\tau + \Delta/s} = \sqrt{12}\sqrt{\frac{\nu''}{(\nu')^2} - 1} \tag{66}$$

The relative width calculated in the time-domain also represents the relative width of the (logarithmic) stretch distribution:

$$\Delta_{\mathrm{rel}} \equiv \frac{y(\tau + \Delta) - y(\tau)}{y(\tau + \Delta/2)}. \tag{67}$$

Upon approaching the strain rate where the mean stretch diverges, i.e., at $\mathrm{Wi}^{\mathrm{sticky}} = 1$, the relative width of the front diverges as $\Delta_{\mathrm{rel}} \approx \sqrt{24p\mathrm{Wi}\mathrm{Wi}^{\mathrm{sticky}}/(1-\mathrm{Wi}^{\mathrm{sticky}})}$. In this equation, the bare Weissenberg number is $\mathrm{Wi} = \mathrm{Wi}^{\mathrm{sticky}}(1-p)\tau_{\mathrm{R}}/\tau_{\mathrm{s}}$. Hence, if the sticker lifetime is $\tau_{\mathrm{s}} = 10\tau_{\mathrm{R}}$ and the fraction of closed stickers is $p = 0.9$ (as in our simulations), then significant broadening of the front only happens very close to the stretch transition: $\mathrm{Wi}^{\mathrm{sticky}} > 0.99$. This verifies that our approximation of a narrow front is indeed accurate.

C. Power-law regression

To determine the sticky Rouse diffusivity, D_{SR}, from the mean-square displacement of the centre of mass

$$\ln \mathrm{MSD} = \ln(6D_{\mathrm{SR}}) + \ln t \tag{68}$$

as a function of time t, and the stretch exponent, ν, from the probability distribution

$$\ln P = c + \nu \ln \lambda \tag{69}$$

as a function of the stretch ratio, λ, we write both equations in the form

$$y = a + bx \tag{70}$$

and perform common linear regression. However, because both power-laws represent asymptotic behaviour for large x, there is also a cutoff value, x_{cutoff}, above which they apply. We determine the cutoff by minimising

$$\chi^2(a,b,i_0) \equiv \frac{1}{N_{\mathrm{data}}+1-i_0-N_{\mathrm{par}}} \sum_{i=i_0}^{N_{\mathrm{data}}} \frac{(y_i^{\mathrm{data}} - y_i^{\mathrm{fit}}(a,b))^2}{\sigma_i^2}, \tag{71}$$

with respect to a, b and i_0 (note that $x_{i_0} = x_{\mathrm{cutoff}}$); σ_i is the uncertainty on the simulated y data. Here, we set $b = 1$ fixed and the number of free parameters $N_{\mathrm{par}} = 1$ for extracting the sticky Rouse diffusivity from the MSD data. To determine the stretch exponent (ν) from the stretch distributions we use the same approach, but leave b as a free fitting parameter and set $N_{\mathrm{par}} = 2$.

ACKNOWLEDGMENTS

This research was funded by the Engineering and Physical Sciences Research Council [grant number EPSRC (EP/N031431/1)]. C.S. is grateful for the computational support

from the University of York high-performance computing service (the Viking Cluster), and thanks Daniel J. Read for his suggestion to pair closed stickers of different chains. C.S. and T.C.B.M. thank Pete Laity and Chris Holland for useful discussions on the mechanism of silk self-assembly.

REFERENCES

[1]R. S. Graham and P. D. Olmsted, "Coarse-grained simulations of flow-induced nucleation in semicrystalline polymers," Phys. Rev. Lett. **103**, 115702 (2009).

[2]E. M. Troise, H. J. M. Caelers, and G. W. M. Peters, "Full characterization of multiphase, multimorphological kinetics in flow-induced crystallization of ipp at elevated pressure," Macromolecules **50**, 3868–3882 (2017).

[3]D. A. Nicholson and G. C. Rutledge, "An assessment of models for flow-enhanced nucleation in an n-alkane melt by molecular simulation," J. Rheol. **63**, 465–475 (2019).

[4]S. Moghadamand, I. S. Dalal, and R. G. Larson, "Unraveling dynamics of entangled polymers in strong extensional flows," Macromolecules **52**, 1296–1307 (2019).

[5]R. S. Graham, "Understanding flow-induced crystallization in polymers: A perspective on the role of molecular simulations," J. Rheol. **63**, 203–214 (2019).

[6]D. J. Read, C. McIlroy, C. Das, O. G. Harlen, and R. S. Graham, "Polystrand model of flow-induced nucleation in polymers," Phys. Rev. Lett. **124**, 147802 (2020).

[7]C. Holland, F. Vollrath, A. J. Ryan, and O. O. Mykhaylyk, "Silk and synthetic polymers: reconciling 100 degrees of separation," Adv. Mater. **24**, 105–109 (2012).

[8]P. R. Laity, E. Baldwin, and C. Holland, "Changes in silk feedstock rheology during cocoon construction: the role of calcium and potassium ions," Macromol. Biosci. **0**, 1800188 (2018).

[9]C. Schaefer, P. R. Laity, C. Holland, and T. C. B. McLeish, "Silk protein solution: A natural example of sticky reptation," Macromolecules **53**, 2669–2676 (2020).

[10]C. Schaefer and T. C. B. McLeish, "Power-law stretching of associating polymers in steady-state extensional flow," Phys. Rev. Lett. **126**, 057801 (2021).

[11]C. Schaefer, P. R. Laity, C. Holland, and T. C. B. McLeish, "Stretching of bombyx mori silk protein in flow," Molecules **26**, 1663 (2021).

[12]T. Asakura, "Structure of silk i (bombyx mori silk fibroin before spinning)-type ii -turn, not -helix-," Molecules **26**, 3706 (2021).

[13]G. J. Dunderdale, S. J. Davidson, A. J. Ryan, and O. O. Mykhaylyk, "Flow-induced crystallisation of polymers from aqueous solution," Nat. Comm. **11**, 3372 (2020).

[14]P. R. Laity and C. Holland, "Seeking solvation: Exploring the role of protein hydration in silk gelation," Molecules **25**, 551 (2020).

[15]S. Donets and J.-U. Sommer, "Molecular dynamics simulations of strain-induced phase transition of poly(ethylene oxide) in water," J. Phys. Chem. B **122**, 392 (2018).

[16]S. Donets, O. Guskova, and J.-U. Sommer, "Flow-induced formation of thin peo fibres in water and their stability after the strain release," J. Phys. Chem. B **124**, 9224 (2020).

[17]S. Donets, O. Guskova, and J.-U. Sommer, "Searching for aquamelt behavior among silklike biomimetics during fibrillation under flow," J. Phys. Chem. B **125**, 3238 (2021).

[18]W. D. Mkandawire and S. T. Milner, "Simulated osmotic equation of state for poly(ethylene oxide)solutions predicts tension-induced phase separation," Macromolecules **54**, 3613 (2021).

[19]L. Leibler, M. Rubinstein, and R. H. Colby, "Dynamics of reversible networks," Macromolecules **24**, 4701–4707 (1991).

[20]R. H. Colby, X. Zheng, M. H. Rafailovich, J. Sokolov, D. G. Peiffer, S. A. Schwarz, Y. Strzhemechny, and D. Nguyen, "Dynamics of lightly sulfonated polystyrene ionomers," Phys. Rev. Lett. **81**, 3876–3879 (1998).

[21]S. Hackelbusch, T. Rossow, P. van Assenbergh, and S. Seiffert, "Chain dynamics in supramolecular polymer networks," Macromolecules **46**, 6273–6286 (2013).

[22]Q. Chen, Z. Zhang, and R. H. Colby, "Viscoelasticity of entangled random polystyrene ionomers," J. Rheol. **60**, 1031–1040 (2016).

[23]T. Tomkovic and S. G. Hatzikiriakos, "Nonlinear rheology of poly(ethylene-co-methacrylic acid) ionomers," J. Rheol. **62**, 1319–1329 (2018).

[24]Z. Zhang, Q. Chen, and R. H. Colby, "Dynamics of associative polymers," Soft Matter **14**, 2961–2977 (2018).

[25]Z. R. Hinton, A. Shabbir, and N. J. Alvarez, "Dynamics of supramolecular self-healing recovery in extension," Macromolecules **52**, 2231–2242 (2019).

[26]M. Golkaram and K. Loos, "A critical approach to polymer dynamics in supramolecular polymers," Macromolecules **52**, 9427–9444 (2019).

[27]M. Zuliki, S. Zhang, K. Nyamajaro, T. Tomkovic, and S. G. Hatzikiriakos, "Rheology of sodium and zinc ionomers: Effects of neutralization and valency," Phys. Fluids **32**, 023104 (2020).

[28]S. Liu, X. Cao, C. Huang, R. A. Weiss, Z. Zhang, and Q. Chen, "Brittle-to-ductile transition of sulfonated polystyrene ionomers," ACS. Macro. Lett. **10**, 503–509 (2021).

[29]T. Witten, "Associating polymers and shear thickening," J. Phys. France **49**, 1055–1063 (1988).

[30]H.-J. Jin and D. L. Kaplan, "Mechanism of silk processing in insects and spiders," Nature **424**, 1057–1061 (2003).

[31]F. Tanaka, R. Takeda, and K. Tsurusaki, "Critical shear rate for gelation in aqueous solutions of associating polymers under shear flows," J. Phys. Soc. Jpn. **87**, 074801 (2018).

[32]Y. Séréro, V. Jacobsen, and J.-F. Berret, "Evidence of nonlinear chain stretching in the rheology of transient networks," Macromolecules **33**, 1841–1847 (2000).

[33]A. Tripathi, K. C. Tam, and G. H. McKinley, "Rheology and dynamics of associative polymers in shear and extension: Theory and experiments," Macromolecules **39**, 1981–1999 (2006).

[34]A. Koeppel, N. Stehling, C. Rodenburg, and C. Holland, "Spinning beta silks requires both ph activation and extensional stress," Adv. Func. Mater. **31**, 2103295 (2021).

[35]H. Janeschitz-Kriegl, "How to understand nucleation in crystallizing polymer melts under real processing conditions," Colloid. Polym. Sci. **281**, 1157–1171 (2003).

[36]O. O. Mykhaylyk, P. Chambon, R. S. Graham, J. Patrick, A. Fairclough, P. D. Olmsted, and A. J. Ryan, "The specific work of flow as a criterion for orientation in polymer crystallization," Macromolecules **41**, 1901–1904 (2008).

[37]J. Seo, A. M. Gohn, R. P. Schaake, D. Parisi, A. M. Rhoades, and R. H. Colby, "Shear flow-induced crystallization of poly(ether ether ketone)," Macromolecules **3472–3481**, 53 (2020).

[38]A. E. Likhtman and T. C. B. McLeish, "Quantitative theory for linear dynamics of linear entangled polymers," Macromolecules **35**, 6332–6343 (2002).

[39]R. S. Graham, A. E. Likhtman, T. C. B. McLeish, and S. T. Milner, "Microscopic theory of linear, entangled polymer chains under rapid deformation including chain stretch and convective constraint release," J. Rheol. **47**, 1171–1200 (2003).

[40]M. H. N. Sefiddashti, B. J. Edwards, and B. Khomami, "Individual chain dynamics of a polyethylene melt undergoing steady shear flow," J. Rheol. **59**, 119 (2015).

[41]M. Mohagheghi and B. Khomami, "Elucidating the flow-microstructure coupling in the entangled polymer melts. part i: Single chain dynamics in shear flow," J. Rheol. **60**, 849–859 (2016).

[42]M. Mohagheghi and B. Khomami, "Elucidating the flow-microstructure coupling in the entangled polymer melts. part ii: Molecular mechanism of shear banding," J. Rheol. **60**, 861–872 (2016).

[43]Q. Huang, J. Ahn, D. Parisi, T. Chang, O. Hassager, S. Panyukov, M. Rubinstein, and D. Vlassopoulos, "Unexpected stretching of entangled ring macromolecules," Phys. Rev. Lett. **122**, 208001 (2019).

[44]T. C. O'Connor, T. Ge, M. Rubinstein, and G. S. Grest, "Topological linking drives anomalous thickening of ring polymers in weak extensional flows," Phys. Rev. Lett. **124**, 027801 (2020).

[45]A. Bonato, D. Marenduzzo, and D. Michieletto, "Simplifying topological entanglements by entropic competition of slip-links," Phys. Rev. Research **3**, 043070 (2021).

[46]P. G. Khalatur and D. A. Mologin, "Rheologlcal properties of self-associating polymer systems: Nonequilibrium molecular dynamics simulation," J. Mol. Liq. **91**, 205–217 (2001).

[47]S. Mohottalalage, M. Senanayake, T. O'Connor, G. Grest, and D. Perahia, "Nonlinear elongation flows effects on aggregation in associating polymer melts," Bull. Am. Phys. Soc. (2021).

[48]M. E. Shivokhin, T. Narita, L. Talini, A. Habicht, S. Seiffert, T. Indei, and J. D. Schieber, "Interplay of entanglement and association effects on the dynamics of semidilute solutions of multisticker polymer chains," J. Rheo. **61**, 1231–1241 (2017).

[49]V. A. H. Boudara and D. J. Read, "Stochastic and preaveraged nonlinear rheology models for entangled telechelic starpolymers," J. Rheol. **61**, 339–362 (2017).

[50]G. Cui, V. A. H. Boudara, Q. Huang, G. P. Baeza, A. J. Wilson, O. Hassager, D. J. Read, and J. Mattsson, "Linear shear and nonlinear extensional rheology of unentangled supramolecular side-chain polymers," J. Rheol. **62**, 1155–1174 (2018).

[51]C. C. Hua and J. D. Schieber, "Segment connectivity, chain-length breathing, segmental stretch, and constraint release in reptation models. i. theory and single-step strain predictions." J. Chem. Phys. **109**, 10018 (1998).

[52]S. Shanbhag, R. Larson, J.-I. Takimoto, and M. Doi, "Deviations from dynamic dilution in the terminal relaxation of star polymers." Phys. Rev. Lett. **87**, 195502 (2001).

[53]M. Doi and J.-I. Takimoto, "Molecular modelling of entanglement." Philos. Trans. R. Soc. **361**, 641–652 (2003).

[54]J. D. Schieber, J. Neergaard, and S. Gupta, "A full-chain, temporary network model with sliplinks, chain-length fluctuations, chain connectivity and chain stretching," J. Rheol. **47**, 213–233 (2003).

[55]A. E. Likhtman, "Single-chain slip-link model of entangled polymers: Simultaneous description of neutron spin-echo, rheology, and diffusion," Macromolecules **38**, 6128–6139 (2005).

[56]M. Andreev and G. C. Rutledge, "A slip-link model for rheology of entangled polymer melts with crystallization," J. Rheol. **64**, 213–222 (2020).

[57]J. M. Dealy, D. J. Read, and R. G. Larson, *Structure and Rheology of Molten Polymers* (Hanser, Munich, 2018).

[58]M. Doi and S. F. Edwards, *The Theory of Polymer Dynamics* (Clarendon, Oxford, 1986).

[59]M. Andreev, R. N. Khaliullin, R. J. A. Steenbakkers, and J. D. Schieber, "Approximations of the discrete slip-link model and their effect on nonlinear rheology predictions," J. Rheo. **57**, 535–557 (2013).

[60]A. Cohen, "A padé approximant to the inverse langevin function," Rheol. Acta **30**, 270–273 (1991).

[61]M. Rubinstein and A. N. Semenov, "Thermoreversible gelation in solutions of associating polymers. 2. linear dynamics," Macromolecules **31**, 1386–1397 (1998).

[62]C. Raffaelli, A. Bose, C. H. M. P. Vrusch, S. Ciarella, T. Davris, N. B. Tito, A. V. Lyulin, W. G. Ellenbroek, and C. Storm, *Rheology, Rupture, Reinforcement and Reversibility: Computational Approaches for Dynamic Network Materials* (Springer, Cham, 2020).

[63]R. Vinu and L. J. Broadbelt, "Unraveling reaction pathways and specifying reaction kinetics for complex systems," Annu. Rev. Chem. Biomol. Eng. **3**, 29–54 (2012).

[64]J. J. Lukkien, J. P. L. Segers, P. A. J. Hilbers, R. J. Gelten, and A. P. J. Jansen, "Efficient monte carlo methods for the simulation of catalytic surface reactions," Physical Review E **58**, 2598–2610 (1998).

[65]K. Binder and D. Heermann, *Monte Carlo Simulation in Statistical Physics*, 5th ed. (Springer-Verlag, Berlin Heidelberg, 2019).

[66]A. P. J. Jansen, *An introduction to kinetic Monte Carlo simulations of surface reactions*, 1st ed. (Springer-Verlag, Berlin Heidelberg, 2012).

[67]J. Ramírez, S. K. Sukumaran, B. Vorselaars, and A. E. Likhtman, "Efficient on the fly calculation of time correlation functions in computer simulations," J. Chem. Phys. **133**, 154103 (2010).

[68]R. M. L. Evans, M. Tassieri, D. Auhl, and T. A. Waigh, "Direct conversion of rheological compliance measurements into storage and loss moduli," Phys. Rev. E **80**, 012501 (2009).

[69]T. F. A. de Greef, M. M. J. Smulders, M. Wolffs, A. P. H. J. Schenning, R. P. Sijbesma, and E. W. Meijer, "Supramolecular polymerization," Chem. Rev. **109**, 5687–5754 (2009).

[70]A. Koeppel, P. R. Laity, and C. Holland, "The influence of metal ions on native silk rheology," Acta Biomaterialia **117**, 204 (2020).

[71]M. Saito and M. Matsumoto, "Simd-oriented fast mersenne twister: a 128-bit pseudorandom number generator," in *Monte Carlo and Quasi-Monte Carlo Methods 2006*, edited by A. Keller, S. Heinrich, and H. Niederreiter (Springer Berlin Heidelberg, Berlin, Heidelberg, 2008) pp. 607–622.

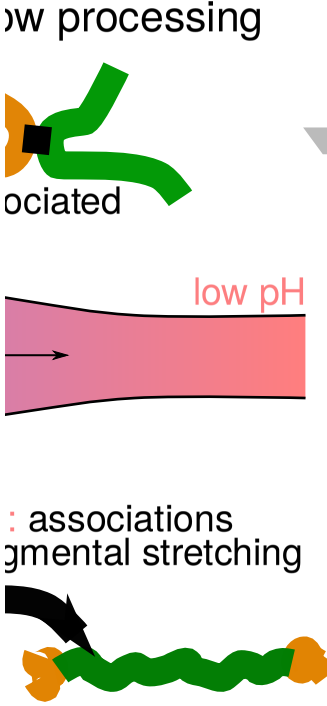
ow processing
ociated
low pH
: associations
gmental stretching

πάντα ῥεῖ

Journal of Rheology

ACCEPTED MANUSCRIPT

PLEASE CITE THIS ARTICLE AS DOI: 10.1122/8.0000411

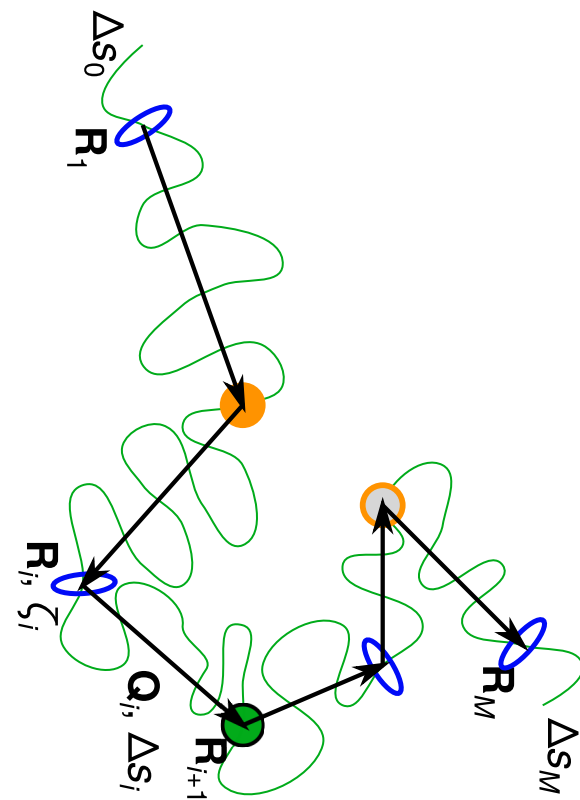

Journal of Rheology

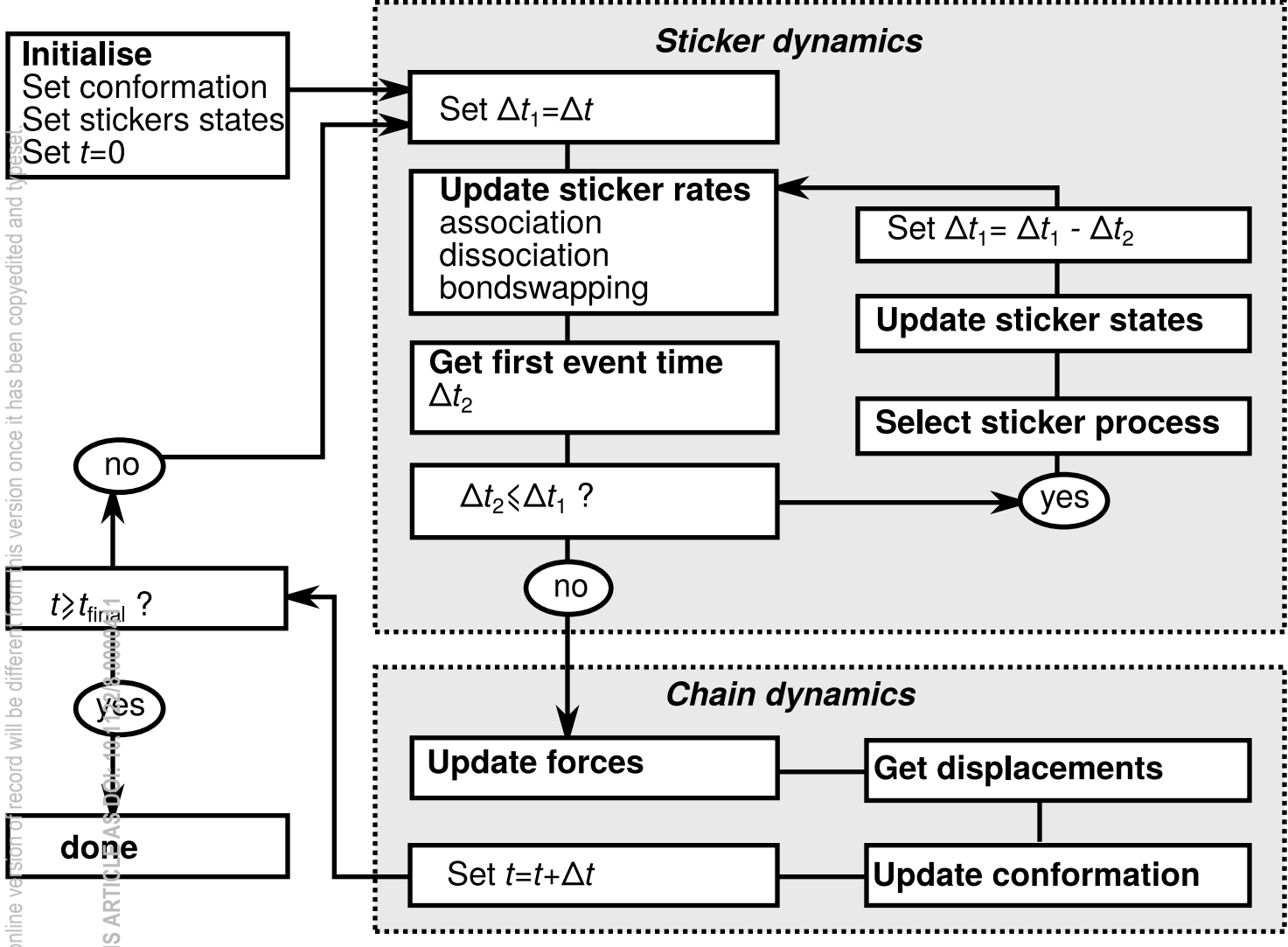

πάντα ῥεῖ

Journal of Rheology

ACCEPTED MANUSCRIPT

PLEASE CITE THIS ARTICLE AS DOI: 10.1122/8.0000411

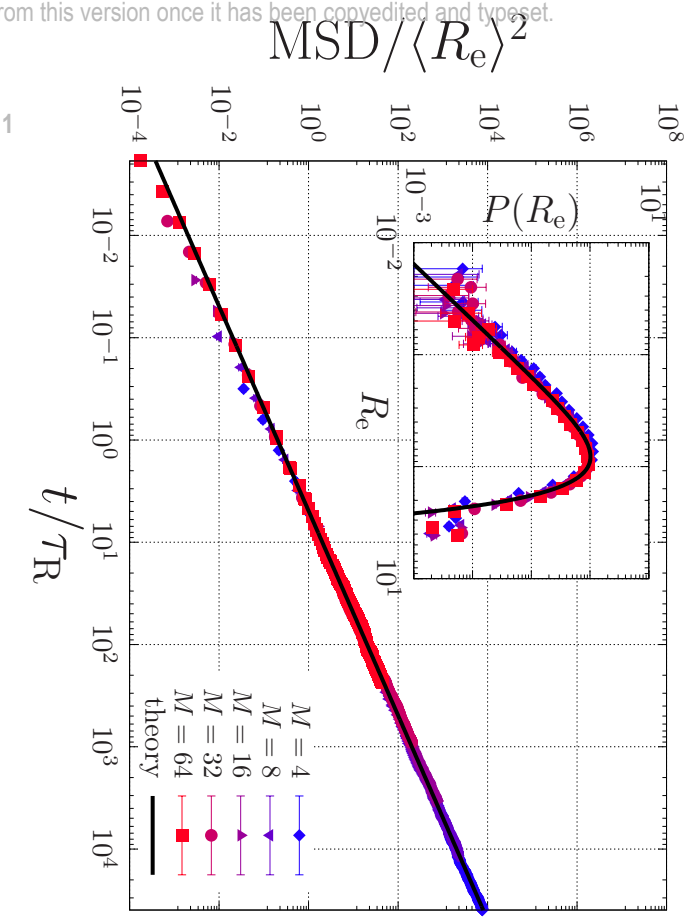

Journal of Rheology ACCEPTED MANUSCRIPT

PLEASE CITE THIS ARTICLE AS DOI: 10.1122/8.0000411

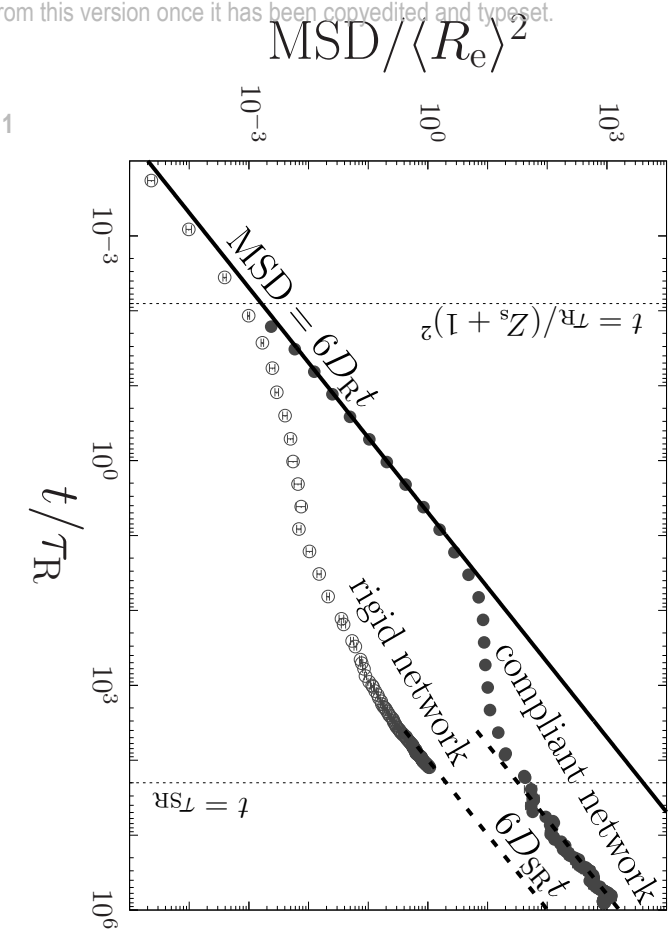

Journal of Rheology

PLEASE CITE THIS ARTICLE AS DOI: 10.1122/8.0000411

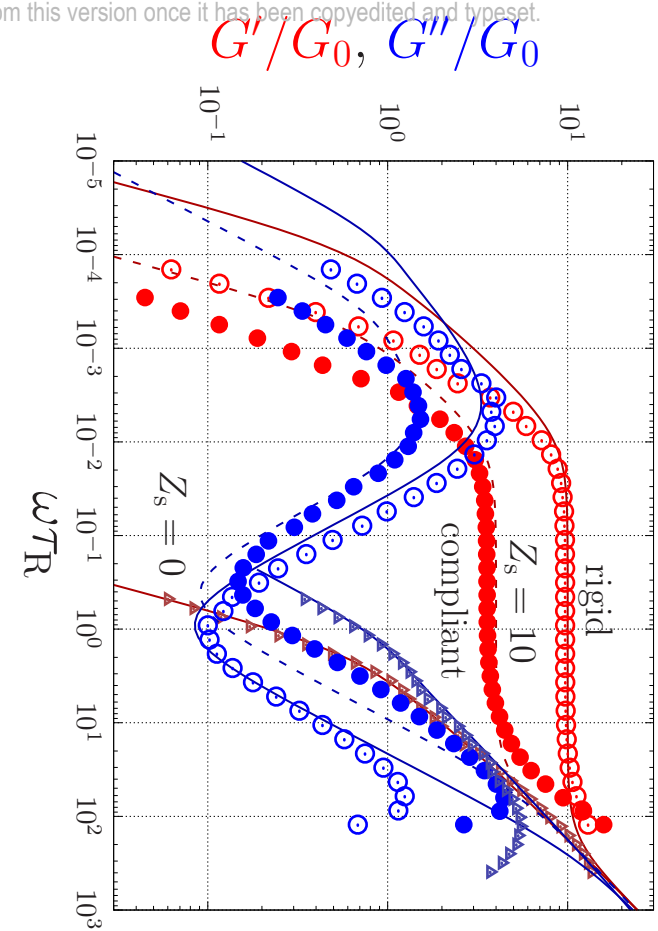

πάντα ῥεῖ

Journal of Rheology

ACCEPTED MANUSCRIPT

PLEASE CITE THIS ARTICLE AS DOI: 10.1122/8.0000411

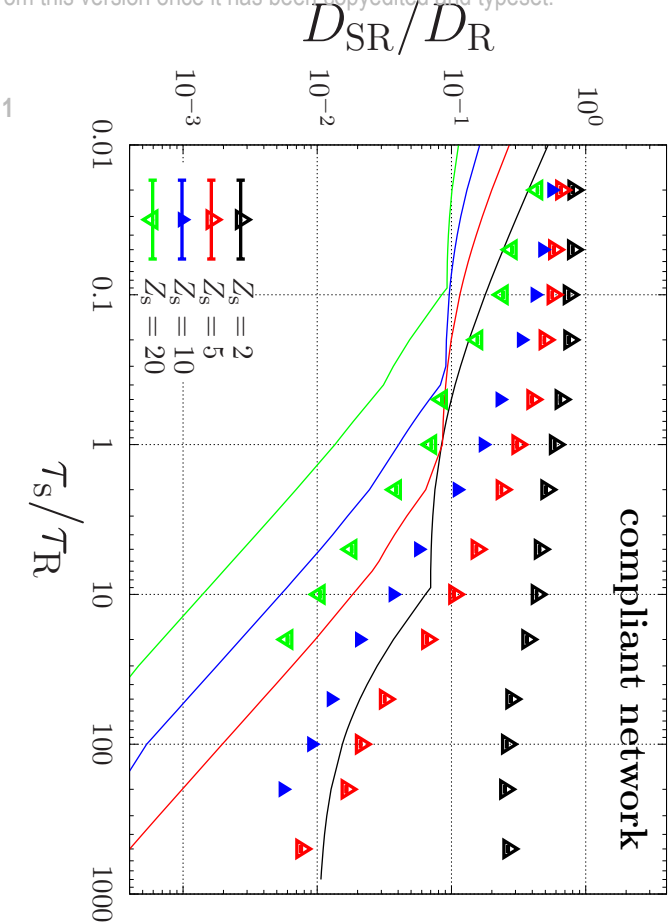

πάντα ῥεῖ

Journal of Rheology

ACCEPTED MANUSCRIPT

PLEASE CITE THIS ARTICLE AS DOI: 10.1122/8.0000411

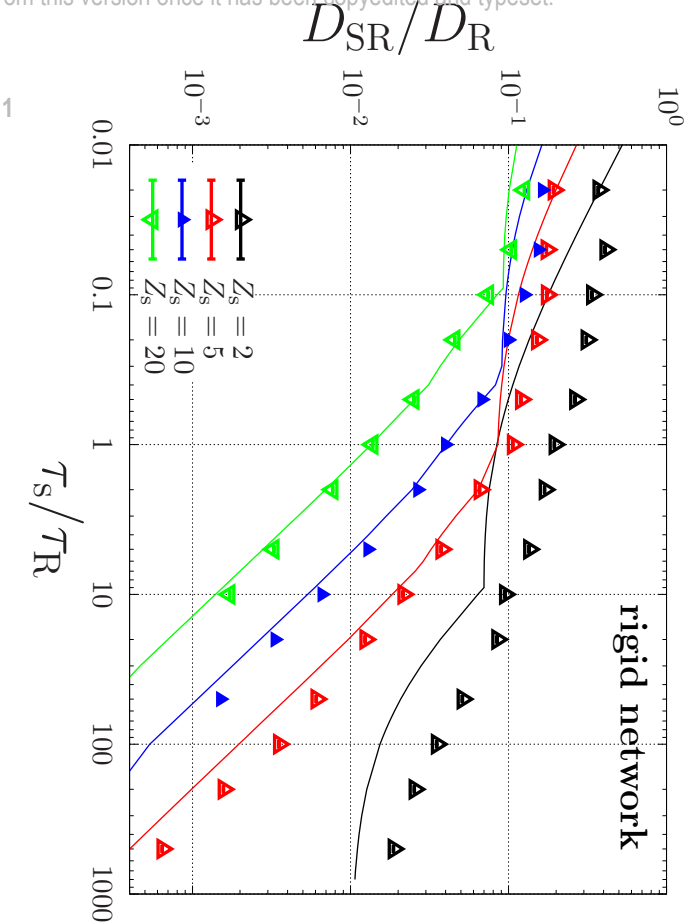

πάντα ῥεῖ

Journal of Rheology

ACCEPTED MANUSCRIPT

PLEASE CITE THIS ARTICLE AS DOI: 10.1122/8.0000411

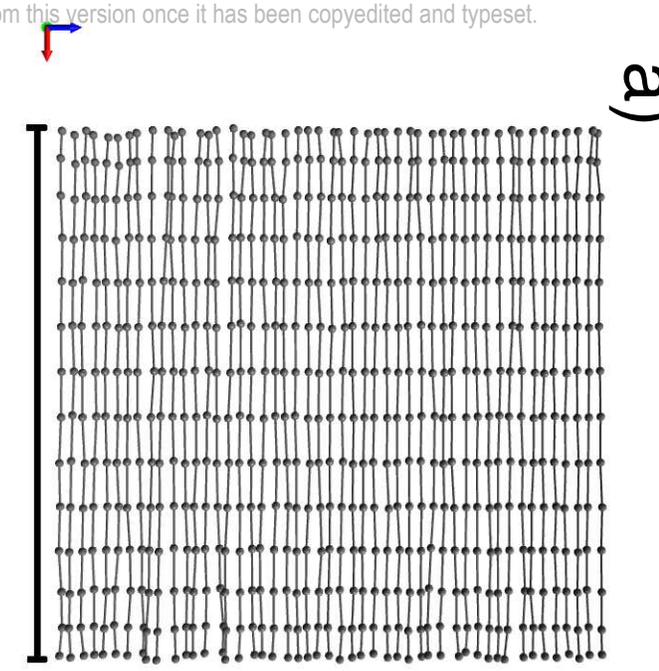

(a)

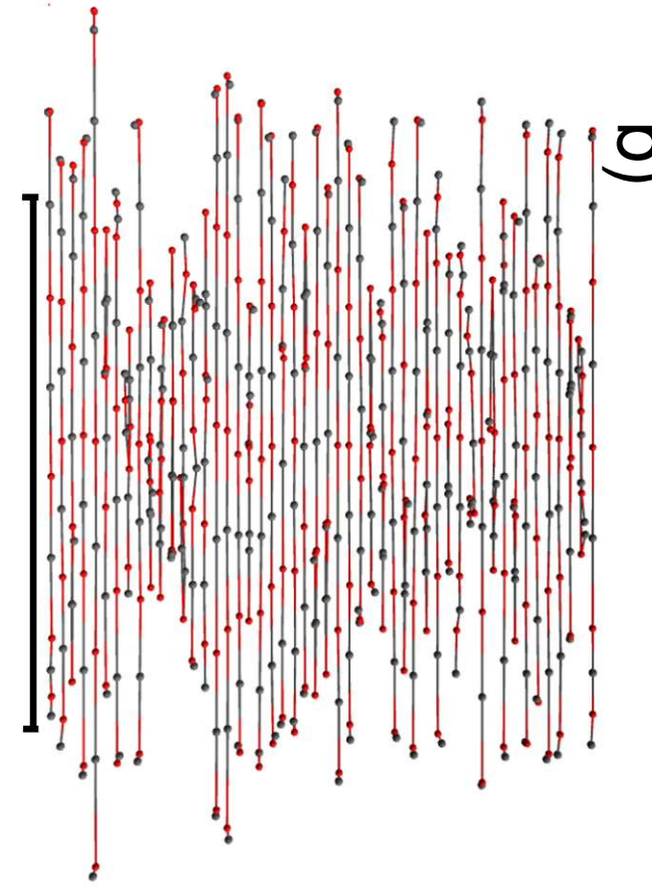

(b)

πάντα ῥεῖ

Journal of Rheology

ACCEPTED MANUSCRIPT

PLEASE CITE THIS ARTICLE AS DOI: 10.1122/8.0000411

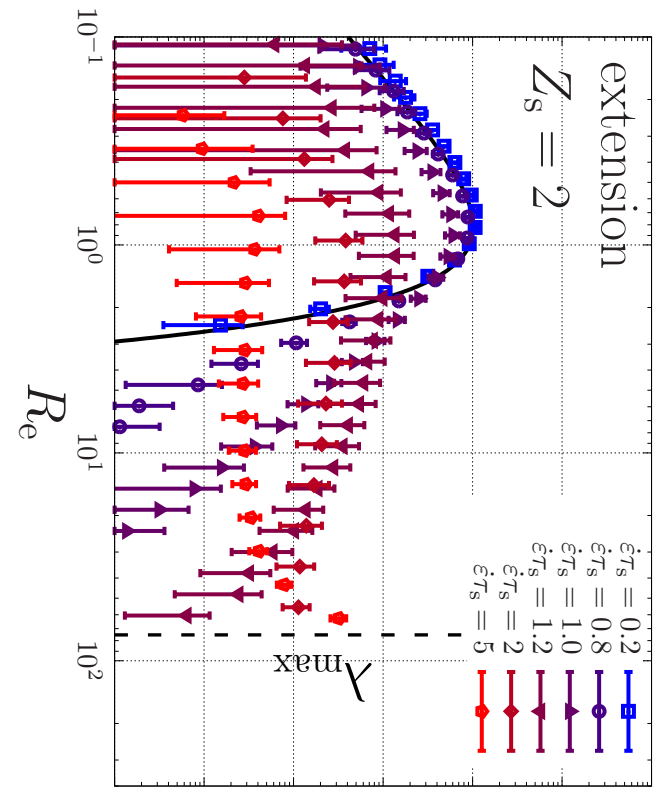

Journal of Rheology

PLEASE CITE THIS ARTICLE AS DOI: 10.1122/8.0000411

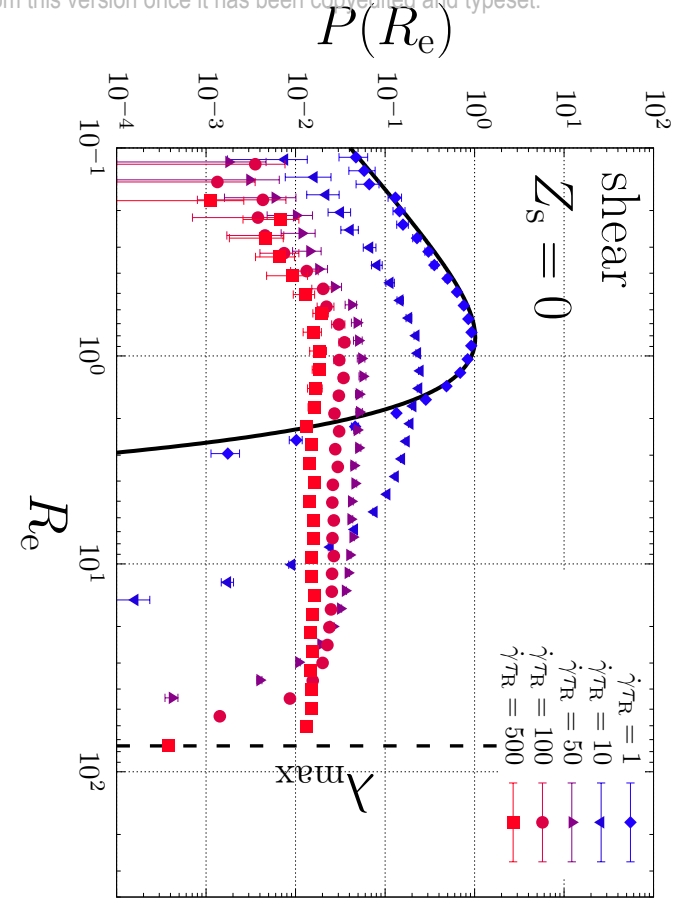

Journal of Rheology ACCEPTED MANUSCRIPT

PLEASE CITE THIS ARTICLE AS DOI: 10.1122/8.0000411

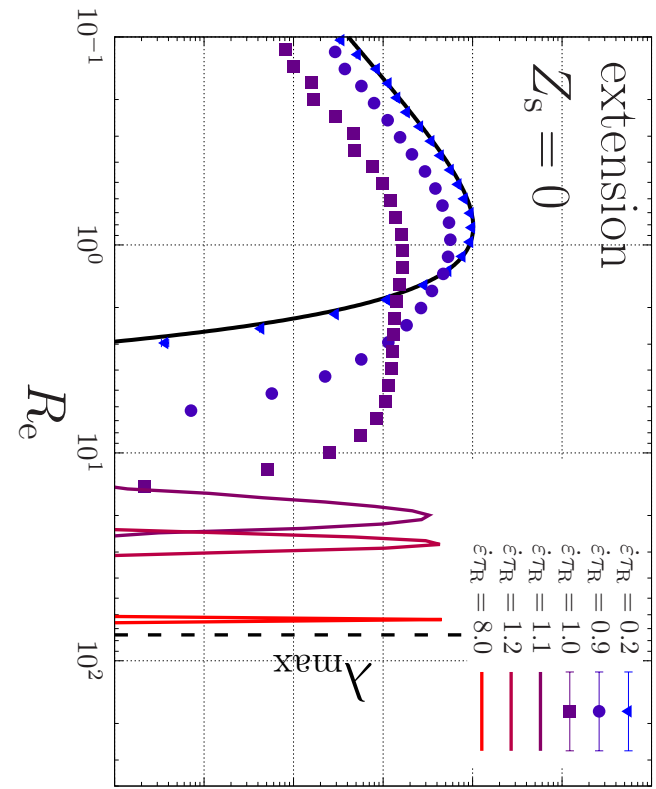

πάντα ῥεῖ

Journal of Rheology

ACCEPTED MANUSCRIPT

PLEASE CITE THIS ARTICLE AS DOI: 10.1122/8.0000411

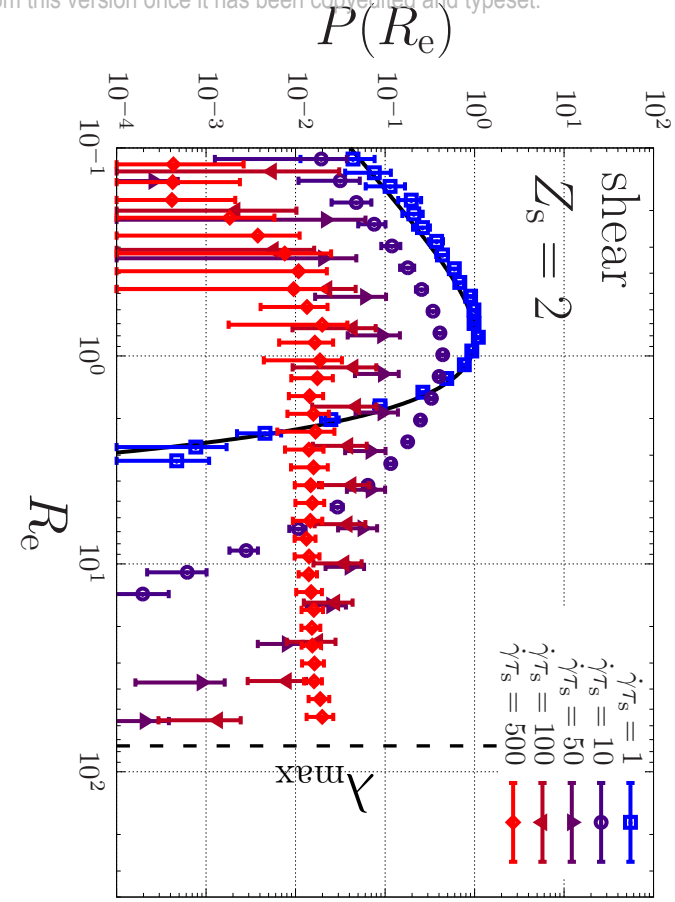

Journal of Rheology

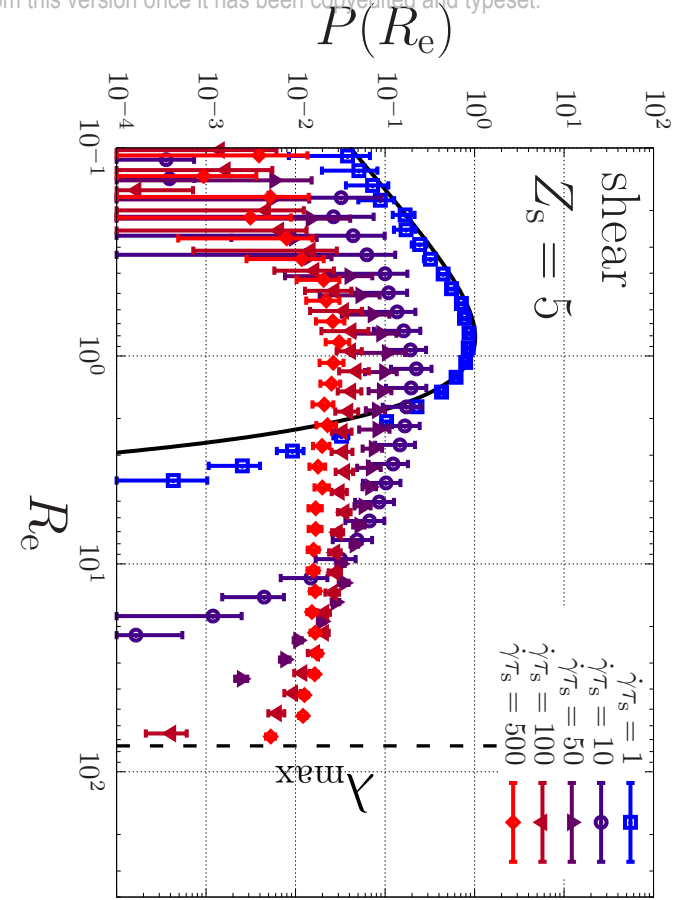

πάντα ῥεῖ

Journal of Rheology

ACCEPTED MANUSCRIPT

PLEASE CITE THIS ARTICLE AS DOI: 10.1122/8.0000411

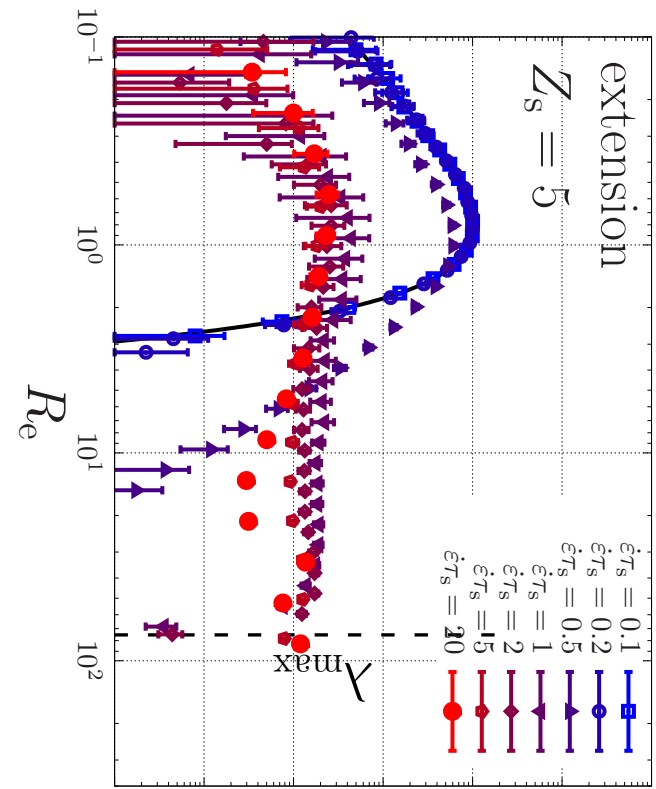

πάντα ῥεῖ

Journal of Rheology

ACCEPTED MANUSCRIPT

PLEASE CITE THIS ARTICLE AS DOI: 10.1122/8.0000411

πάντα ῥεῖ

Journal of Rheology

ACCEPTED MANUSCRIPT

PLEASE CITE THIS ARTICLE AS DOI: 10.1122/8.0000411

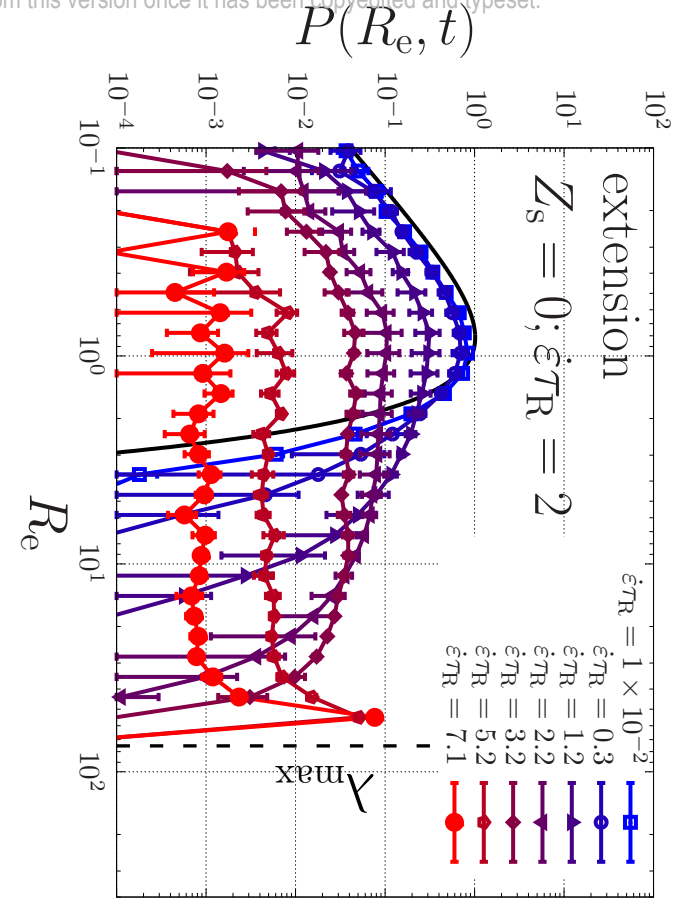

Journal of Rheology

PLEASE CITE THIS ARTICLE AS DOI: 10.1122/8.0000411

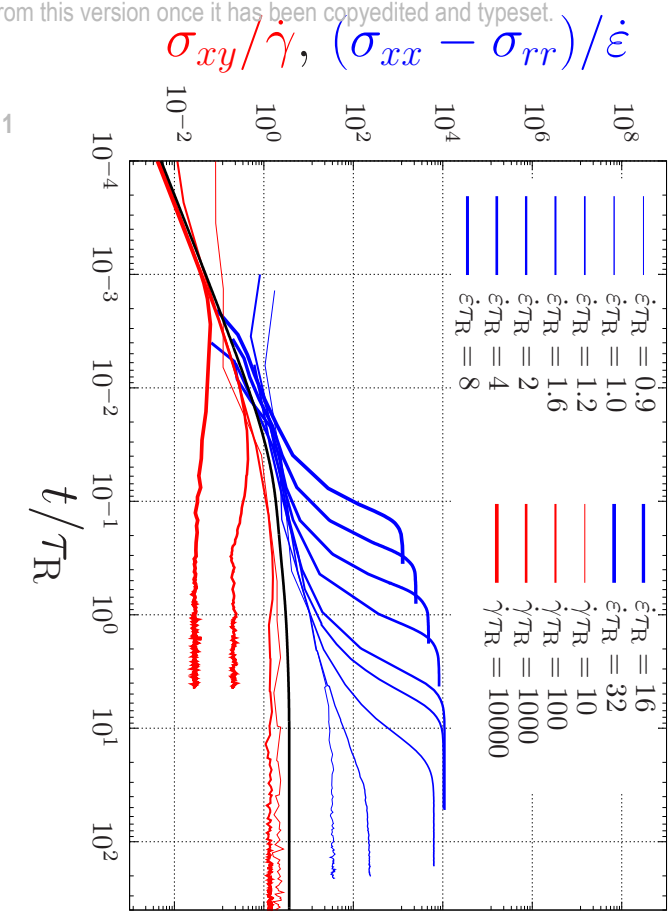

πάντα ῥεῖ

Journal of Rheology

ACCEPTED MANUSCRIPT

PLEASE CITE THIS ARTICLE AS DOI: 10.1122/8.0000411

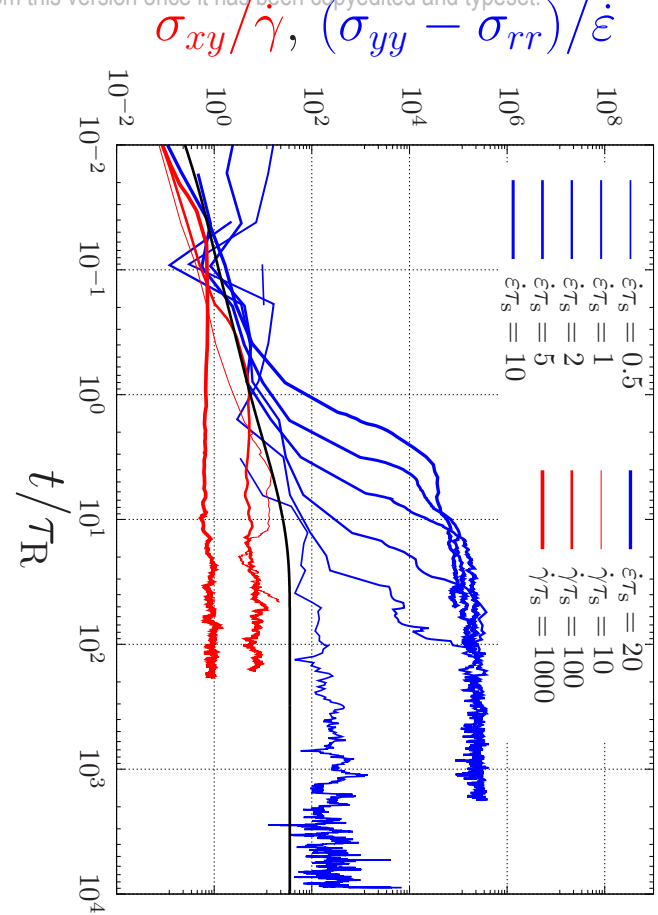

Journal of Rheology

PLEASE CITE THIS ARTICLE AS DOI: 10.1122/8.0000411

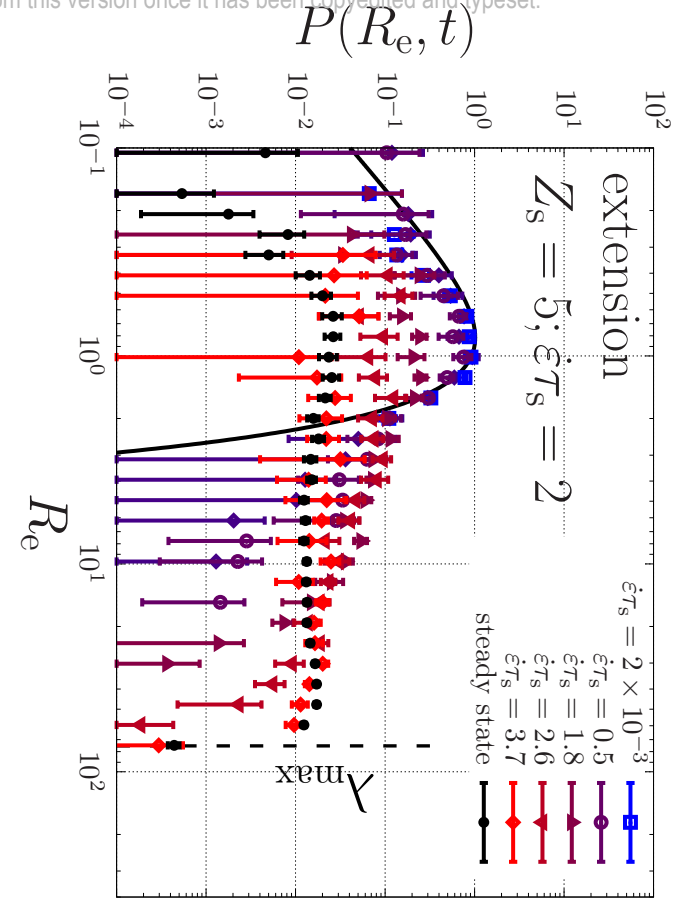

πάντα ῥεῖ

Journal of Rheology

ACCEPTED MANUSCRIPT

PLEASE CITE THIS ARTICLE AS DOI: 10.1122/8.0000411

πάντα ῥεῖ

Journal of Rheology

ACCEPTED MANUSCRIPT

PLEASE CITE THIS ARTICLE AS DOI: 10.1122/8.0000411

Journal of Rheology

PLEASE CITE THIS ARTICLE AS DOI: 10.1122/8.0000411

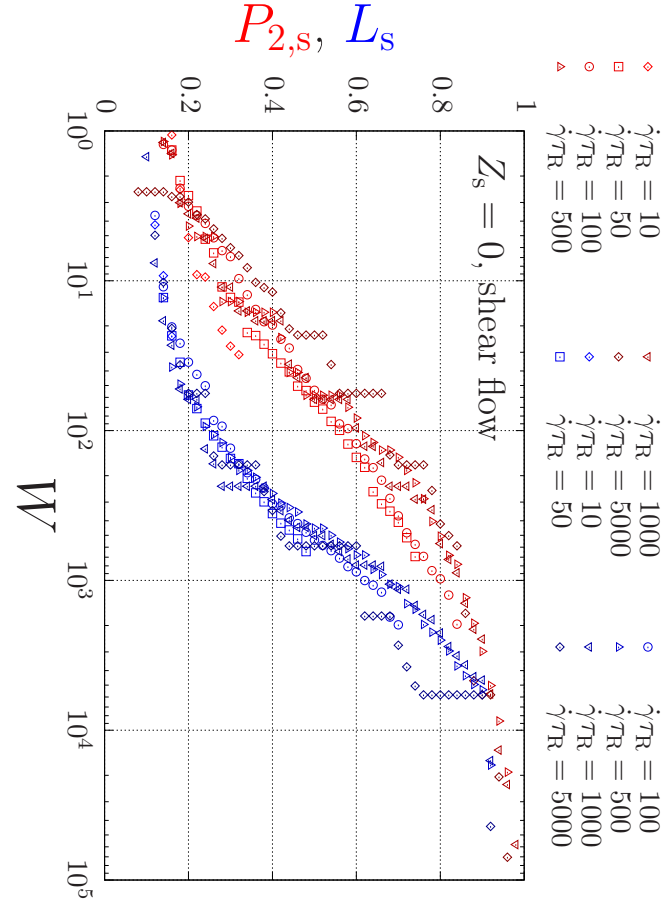

πάντα ῥεῖ

Journal of Rheology

ACCEPTED MANUSCRIPT

PLEASE CITE THIS ARTICLE AS DOI: 10.1122/8.0000411

Journal of Rheology

PLEASE CITE THIS ARTICLE AS DOI: 10.1122/8.0000411

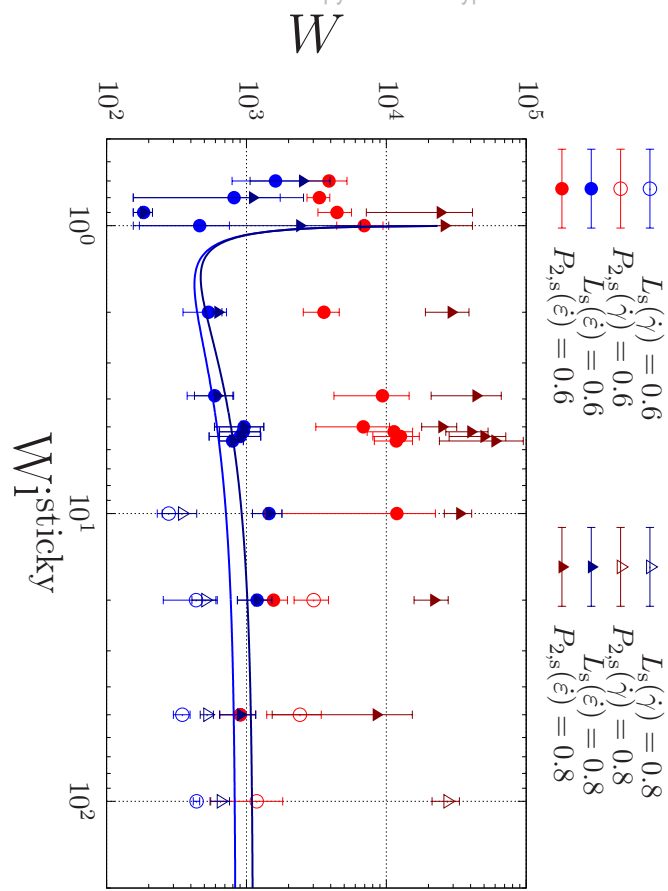

Journal of Rheology

PLEASE CITE THIS ARTICLE AS DOI: 10.1122/8.0000411